Tampereen yliopisto

Taneli Leppänen

THRUSTER DRIVELINE DIGITAL TWIN

Bearing and Shaft Fatigue Life Prediction

Faculty of Engineering Sciences
Master's Thesis
May 2021

ABSTRACT

Taneli Leppänen: Thruster Driveline Digital Twin – Bearing and Shaft Fatigue Life Prediction
Master's Thesis
Tampere University
Master's Degree for Mechanical Engineering
May 2021

In the most basic form, drivelines consist of combination of shafts, gearboxes and clutches to transit and transform the torque and of bearing for support. Continuous and predictable operation is key for profitable operation of most commercial assets, ships and their thrusters included. Life-time predictions and maintenance schedules are of based on calculation made in the design stages of the asset or on general recommendation from the manufacturer. These design stage calculations usually rely on conservative estimation of the usage profile or past experiences, if those are available, resulting in the best case in premature replacement of components or in the worst case in unexpected failure, both of which can be costly.

One way to alleviate this mismatch between expectations and real operation is to setup a condition monitoring scheme which can be further enhanced with real time calculations based on the measured data to predict component failures. This kind of real time data based calculation system can be collegially referred as a digital twin. With our load based lifetime predictions we can setup a condition based maintenance scheme, where maintenance can planed according to actual component condition.

For the scope of the thesis bearing and shaft calculation packages were chosen to be implemented in Python 3. The calculations were based on DIN 743 for shaft, and ISO 281 and ISO TS 16281 for bearings. The approach of using standardized methodologies was chosen for two reasons. Firstly, Kongsberg has experience using all of these standards and secondly, many of the maritime classification societies recognize these standards, which makes classification of the digital twin system easier.

With the shaft calculation package, generating valid for the standard calculation proved difficult due to the method requiring the load to be inputted in three different directions where the rainflow counting routines usually only can analyze a signal from a single direction. To account for this a synchronization scheme was implemented, but a more specialized multidirectional counting routine should be further investigated. The shaft stress calculation match well with the reference commercial implantation, but fatigue damage results should be further verified since the reference program only outputs safety factors.

For bearing calculations, the computation on of the contact stresses between the rolling element and the bearing ring proved most difficult. The difficulties came down to unavailability of the bearing inner geometries, which manufactures consider proprietary information. Due to lack of information verification of the bearing module proved difficult since separation between errors introduced by incorrect inputs and possible errors in the implementation is not possible. To circumvent this issue, generation of the pressure distributions by the manufactures to generate a ROM model should be investigated.

Keywords: digital twin, driveline, bearing, shaft, fatigue, condition monitoring, predictive maintenance, ISO 281, ISO TS 16281, DIN 743

TIIVISTELMÄ

Taneli Leppänen: Thruster Driveline Digital Twin – Bearing and Shaft Fatigue Life Prediction
Diplomityö
Tampereen yliopisto
Konetekniikan DI-tutkinto-ohjelma
Toukokuu 2021

Yksinkertaisimmillaan voimalinja koostuu akseleista, vaihteista ja kytkimistä, jotka siirtävät ja muuntavat vääntöä sekä voimalinjaa tukevista laakereista. Jatkuvuus ja ennustettavuus ovat avainasemassa taloudellisesti kannattassa laitteiden operoinnissa, laivat ja niiden potkurilaitteet mukaanlukien. Komponenttien elinajan ennusteet sekä huoltosuunnitelmat perustuvat usein suunnittelu vaiheessa tehtyihin laskelmiin taikka valmistajan yleisiin ohjeistuksiin. Nämä laskelmat pohjautuvat usein konservatiivisiin oletuksiin käyttöprofiilista tai mahdollisiin aikaisempiin kokemuksiin, mikä johtaa parhaassa tapauksessa komponentin ennenaikaiseen vaihtamiseen tai pahimmassa tapauksessa odottamattomaan rikkoutumiseen, mistä molemmat voivat olla kalliita.

Yksi tapa ehkäistä eroa odotusten ja todellisen operoinnin välillä on sovittaa laitteeseen kunnunvalvonta järjestelmä, jota voidaan tehostaa reaaliaikaisilla laskentamalleilla, jotka pohjautuvat mitattuun, milla voidaan ennustaa kompponenttien rikkoutumista. Tälläistä reaaliaikaista mittadataan pohjautuvaa laskentasysteemiä voidaan yleisesti kutsua digitaaliseksi kaksoseksi. Tuotetuilla mittadataan pohjautuvilla väsymislaskelmilla voidaan implementoida komponentien kuntoon pohjautuva huoltosuunnitelma, jossa komponentit vaihdetaan niiden todelliseen kuntoon pohjautuen.

Tämän diplomityön aiheeksi valittiin laakerien ja akselien laskentamallin toteuttaminen Python 3 -ohjelmointikielellä. Akseli laskentamalli pohjautui DIN 743 standardiin, ja laakeri laskentamalli ISO 281 sekä ISO TS 16281 standardeihin. Standardi pohjaisten laskentamallien kehittämiselle oli kaksi pääsyytä. Ensinäkin, Kongsbergilla on paljon kokemusta mainittujen standardien käytöstä ja toiseksi, monet merenkulun luokituslaitset tunnistavat kyseiset standardardit, joten digitaalisen kaksosen luokittaminen helpottuu huomattavasti.

Akselilaskennassa, standardin määrittämän kuorman syötteen generointi osoittautui hankalaksi, koska se täytyi syöttää kolmena eri suuntana, kun rainflow -laskentarutiini pystyy analysoimaan vain yhtä suuntaa kerrallaan. Tätä varten kehitettiin synkronointi systeemi, mutta tarkemman monisuunta rainflow -laskentarutiin käyttöä tulisi tutkia tulevaisuudessa. Akselilaskennan osana olevat jännitys luvut vastasivat hyvin kaupallisen referenssi ohjelman tuloksia, mutta väsimis vahingon laskentatuloksia ei pystytty tämän diplomityön osana verifioimaan, koska referenssi ohjelmalla pystyttiin laskemaan vain varmuuslukuja.

Laakereiden kohdalla kontaktipaineen laskeminen pyörimiselinten ja kehien välillä osoittautui hakkein haasteellisimmaksi. Laskennan vaikeus johtui laakerein sisäisen geometrian tiedon saatavuudesta, sillä laakerivalmistajat pitävät tätä tietoa salaisena. Tästä johtuen laakeri laskentaa verifioitaessa ei ollut mahdollista erotella huonoista lähtötiedoista ja mahdollisista mallin virheistä johtuvia eroja. Tulvaisuudessa voisi olla mahdollista pyytää valmistajia generoimaan kontaktipaine jakaumia laakereille, joista voisi sitten koota vastepintamallin.

Avainsanat: digitaalinen kaksonen, voimalinja, laakeri, akseli, väsyminen, kunnonvalvonta, ennakoiva huolto, ISO 281, ISO TS 16281, DIN 743

PREFACE

I would like to thank Professor Reijo Kouhia for his guidance on this theses and teaching along the years along with the rest of the staff in Tampere University. Secondly, I want to thank Kongsberg Rauma and in particular Joni Keski-Rahkonen for offering the traineeship and this thesis opportunity along with Samuli Karsikas for their guidance. All of this has projected my professional career on a quite unorthodox route for a mechanical engineer. Lastly, a thank you to my family and friends for support and patience.

Tampereella 12.05.2021

Taneli Leppänen

TABLE OF CONTENTS

FIGURES

TABLES

SYMBOLS AND ABBREVIATIONS

ISO	International Organization for Standardization
DIN	Deutsches Institut für Normung (German Institute for Standardization)
TS	technical specification
rbb	radial ball bearing
rrb	radial roller bearing
tbb	thrust ball bearing
trb	thrust roller bearing
AST	alternative slicing technique
FEM	finite element method
ROM	reduced order model
IoT	Internet of Things
$\sum\rho$	curvature sum
a	half diameter of the herzian contact in major direction, in millimeters
a_1	reliability factor
a_{ISO}	life modification factor for modified bearing life
b_1	factor in bearing modification factor calculation for equivalent load P
b_2, b_3	bearing specific constant in basic dynamic load rating equivalent load calculations
b_m	rating factor used in basic dynamic rating life calculations
b_w	Wöhler curve exponent
C	basic dynamic load rating, in newtons
c_1	load direction specific exponent in basic dynamic load rating equivalent load calculations
C_a	basic dynamic axial load rating, in newtons
C_r	basic dynamic radial load rating, in newtons
C_u	fatigue load limit, in newtons
c_w	constant for Wöhler curve sloped portion
D	damage
d	notch cross section diameter
d_B	reference diameter of a smooth test bar
d_{BK}	notch reference diameter
d_{eff}	effective notch diameter for heat treatment
d_i	inner ring raceway diameter
D_{pw}	bearing pitch diameter, in millimeters
D_w	ball diameter, in millimeters
D_{we}	roller diameter, in millimeters
e	life scatter exponent
E	Young's modulus
F_a	axial component of the applied bearing load, in newtons
f_c	geometrical factor used in basic dynamic rating life calculations
$f_{i,j}$, $w_{i,j}$	influence coefficient
F_r	radial component of the applied bearing load, in newtons
h, c	experimental exponents
i	number of rolling element rows in bearings
k	contact type specific exponent
K	contacts stiffness, in newtons per millimeter
K_1	technological influence factor
K_{2F}	static support factor
$K_{F\sigma}$	influence factor for surface roughness for tension/compression and bending
$K_{F\tau}$	influence factor for surface roughness for torsion
K_i	inner ring contacts stiffness
K_n	combined contacts stiffness
K_o	outer ring contacts stiffness

K_V	influence factor for surface conditioning
K_σ	combined influence factor for tension/compression and bending
K_τ	combined influence factor for torsion
l	length of the raceway in herzian contact major direction
L_{10}	basic rating life, in millions of revolutions
L_n	bearing rating life, in millions of revolutions
L_{nm}	modified basic rating life, in millions of revolutions
L_{nmr}	modified reference rating life, in millions of revolutions
L_{nr}	reference rating life, in millions of revolutions
L_{we}	effective roller length, in millimeters
m, b_0	viscosity ratio range specific factor used in lubrication factor calculation
m_{AST}	exponent specific for inner and outer ring contacts in AST
N	number of cycles, in millions of cycles
n	rotational speed of the bearing, in revolutions per minute
N_C	number of cycles for loading
n_c	number of revolutions
N_D	high cycle fatigue cycle limit
N_L	fatigue cycle limit for loading
N_S	low cycle fatigue cycle limit
n_s	number of laminae
P	equivalent dynamic load, in newtons
p, w	load life exponent
P_a	equivalent dynamic axial load, in newtons
P_d	diameter clearance
P_r	equivalent dynamic radial load, in newtons
Q_c	basic dynamic load rating equivalent load on rolling element
q_c	basic dynamic load rating equivalent load on rolling element for lamina
Q_j	load on rolling element j
$q_{j,k}$	load on roller j lamina k
q_k	load on lamina k
q_{kei}	equivalent load on lamina k, inner ring
q_{keo}	equivalent load on lamina k, outer ring
Q_{max}	maximum rolling element load
Q_ψ	rolling element load at position ψ
S	reliability, in percents
S_C	safety factor
S_S	safety factor matching yield strength
s_n	sensitivity factor for fatigue notch factor
v	operating kinematic viscosity, in square millimeters per second
V	volume
v_1	reference kinematic viscosity, in square millimeters per second
x	coordinate
X	radial loading factor
Y	axial loading factor
Z	number of rolling elements per row
z'	stress-weighted average depth
z_0	depth of the most critical shear stress
α	contact angle
α_0	nominal contact angle
α_σ	stress concentration factor for principal stress
α_τ	stress concentration factor for shear stress
β_σ	fatigue notch factor for tension/compression and bending
β_τ	fatigue notch factor for torsion
γ_F	increase factor for yield point
δ	deformation
δ^*	dimensionless deformation
δ_{max}	maximum deformation in rolling elements
δ_n	combined contact deformation

δ_r	radial ring shift
ε	loading zone factor
η	bearing life factor for stress
η_a	macro stress factor
η_b	lubrication factor
η_c, e_C	contamination factor
κ	viscosity ratio
ν	Poisson's coefficient
ρ	curvature
σ_{bADK}	damaging bending stress amplitude
σ_{bASK}	yield stress amplitude for bending
σ_{bm}	mean bending stress
σ_{bmax}	maximum bending stress
σ_{bFK}	yield point for bending
σ_{bW}	fatigue limit of a smooth bar under reversed stress for bending, in MPa
σ_{bWK}	notch fatigue limit under reversed stress for bending, in MPa
σ_{max}	maximum principal stress at notch
σ_{nom}	nominal principal stress on shaft
σ_S	yield strength
σ_u	fatigue stress limit
σ_{vm}	von Mises mean stress
σ_{zdADK}	damaging tension/compression stress amplitude
σ_{zdASK}	yield stress amplitude for tension/compression
σ_{zdFK}	yield point for tension/compression
σ_{zdm}	mean tension/compression stress
σ_{zdmax}	maximum tension/compression stress
σ_{zdW}	fatigue limit of a smooth bar under reversed stress for tension/compression, in MPa
σ_{zdWK}	notch fatigue limit under reversed stress for tension/compression, in MPa
τ	combined shear stress according to stress criterion
τ_0	critical shear stress
τ_{max}	maximum shear stress at notch
τ_{nom}	nominal shear stress on shaft
τ_{tADK}	damaging torsion stress amplitude
τ_{tASK}	yield stress amplitude for torsion
τ_{tFK}	yield point for torsion
τ_{tm}	mean torsion stress
τ_{tmax}	maximum torsion stress
τ_{tW}	fatigue limit of a smooth bar under reversed stress for torsion, in MPa
τ_{tWK}	notch fatigue limit under reversed stress for torsion, in MPa
τ_u	fatigue stress limit for shear
τ_{vm}	von Mises mean stress shear component
ψ	angular position
ψ_{brg}	bearing specific factor used in lubrication factor calculation
$\psi_{b\sigma K}$	influence factor for mean bending stress sensitivity
ψ_l	loading zone limit angle
$\psi_{zd\sigma K}$	influence factor for mean tension/compression stress sensitivity
$\psi_{\tau K}$	influence factor for mean torsion stress sensitivity

1. INTRODUCTION

Goal of this thesis was to develop fatigue damage calculation programs for shafts and bearings as part of Kongsbergs thruster digital twin project. The function of these programs was to produce damage values for different components based on continuously measured loading on the driveline. The shaft calculation program was based on DIN 743 standard, and the bearings calculation program was based on ISO 281 standard and ISO 16281 technical specification. These standards were selected because there is a lot of experience in Kongsberg Maritime working with them in the design phases of the azimuthing thruster and were deemed suitable for use in the in-operation condition monitoring. These standards are also widely accepted by different classification societies, which play a key role in acceptance criterions for sea going vessels and their components. The value for such a monitoring system comes from the increased insight given to ship operators to better plan their operations and maintenances.

Both calculation programs were implemented using Python 3 programming language. This was a good fit since the simple syntax of the language allows for quick iteration of the program, which is useful in this sort of new development. Abundance of useful 3rd party packages such as as numpy and rainflow were also utilized to use ready made parts for some sections of the programs. One drawback of Python is that it is a interpreted language which makes it slower compared to compiled languages such as C/C++ and FORTRAN, but this was not a substantial hindrance since most of the computations were symbolic.

In Chapter 2 we take a brief look at some of the concepts regarding the digital twin, namely the digital twin concept itself, different maintenance schemes and fatigue. This includes their development and history to the extent which is of interest to this thesis.

In Chapter 3 we define the bearing calculation mathematically. We go over basic and reference rating life calculation with the modified version of both. Lastly the operation of the program is described briefly.

In Chapter 4 we go over the shaft calculation scheme in the same fashion as it was done for bearings in Chapter 3. In addition, we take a look at rainflow cycle counting needed to get input data for the shaft calculation program. The operation of the program is described in the end.

In Chapter 5 we go over the verification of the created programs and discus the calculated results. The verification of the models is done against tools currently used by Kongsberg in the design processes.

Lastly, in Chapter 6 we present a summary and conclusions of the thesis. Future research is also briefly discussed.

2. DIGITAL TWIN

In this chapter we take a general historical look into digital twins and some related topics, in the case of this thesis, maintenance and fatigue. For digital twins we take a look at their history and role in terms of asset condition monitoring. Following this we describe the various levels of maintenance and how a digital twin of the system can aid in creating a maintenance scheme. Lastly the developmental history of fatigue will be gone over regarding topics related to the thesis.

2.1 Digital Twin

Each of the industrial revolutions have been marked with a substantial leap in technology, leading to huge shifts in the way things are made and operated. The first revolution was brought on by the by the invention of the steam engine in the late 18th century, enabling steam powered machinery and rail transportation [41]. The end of the 19th century marked the second industrial revolution with rapid increases in standardization, steel making and electrification brining about birth of mass manufacturing [42]. At the change of the millennium the Internet was invented and became more widespread enabling fast and affordable information flow across the globe. As a natural continuation to the spread and increased coverage of the Internet, we find more and more systems integrating hardware and software bringing about the industrial internet, more commonly known by the abbreviation IoT (Internet of Things). The birth of the IoT is one of the markers for the start of the fourth industrial revolution or Industry 4.0 [43] p.3 and one the new technologies emerging from it is the digital twin.

Even though the digital twin concept is quite new, the idea of building “twins” dates back to the 60s and 70s and to NASA’s Apollo program. During that time NASA used to build two identical copies of the space bound vehicles, one of which would remain on earth and was referred to as the “twin”. During missions, the twin on earth was fed flight data from the space craft to simulate flight conditions. The twin was used for training purposes, simulate alternative scenarios and assist during missions. [44], p. 63, 64 [45] This was also famously depicted in the 1995 movie Apollo 13.

Another example of the predecessor of the twins are the “iron birds” in the aviation industry. Iron bird is a mockup of the airplane with all of its major components installed with external input and flight conditions generated by simulators. They are used in the design phase for testing and validation of different systems and interactions. During operations these iron birds can be then used for debugging specific issues with the aircraft [44], p. 64 [45] [46]. While computational capabilities are ever increasing, physical components can be replaced by digital ones decreasing costs and removing the requirements for the need a of available physical component [44], p. 64, moving closer to the idea of a true digital twin.

The concept of creating a digital data driven physics based replication of a system is almost 20 years old and it was first suggested by John Vickers of NASA and Michael Grieves of Florida Tech in 2003 [47][48]. The term “digital twin” itself was first defined in a NASA roadmap in 2010 where it called for development of “an integrated multiphysics, multiscale simulation of a vehicle or system that uses the best available physical models, sensor updates, fleet history, etc., to mirror the life of its corresponding flying twin.” [49] p. 5

The twin wasn’t developed only for in-flight monitoring and predictions, but also as an developmental tool [49] p. 22 and it is often suggested that the digital twin should be developed along side the physical twin. By making a digital twin of the product in the developmental phase of the system, engineers are able to better understand complex systems to reduce the number of unknown parameters in the system resulting in a possibility to lower factors of safety [50], usually resulting in a cheaper to manufacture and better performing system. As thing manufactured in the real world are made up to a specific tolerance, meaning things are never perfect and no system is identical to another, the designers can use the digital twin to understand this part of the equation introducing statistic elements into the analysis [49] p. 22, with tools such as Monte Carlo analysis.

Even though the digital twin as a concept is fairly old, the cost of operating such a complex simulation has become manageable only in the recent years. The amount of computational power per cost has exponentially increased and is only predicted to rise [51] p. 86, 87 as seen in Figure 1. Another thing making digital twin more accessible is development of more accurate analytical

models of components, such as ISO TS 16281 for bearings, resulting from a better understanding of the underlying component specific physics. Instead of creating a complex numerical simulation of the component, these cheaper to compute models can be used as was done in this thesis work.

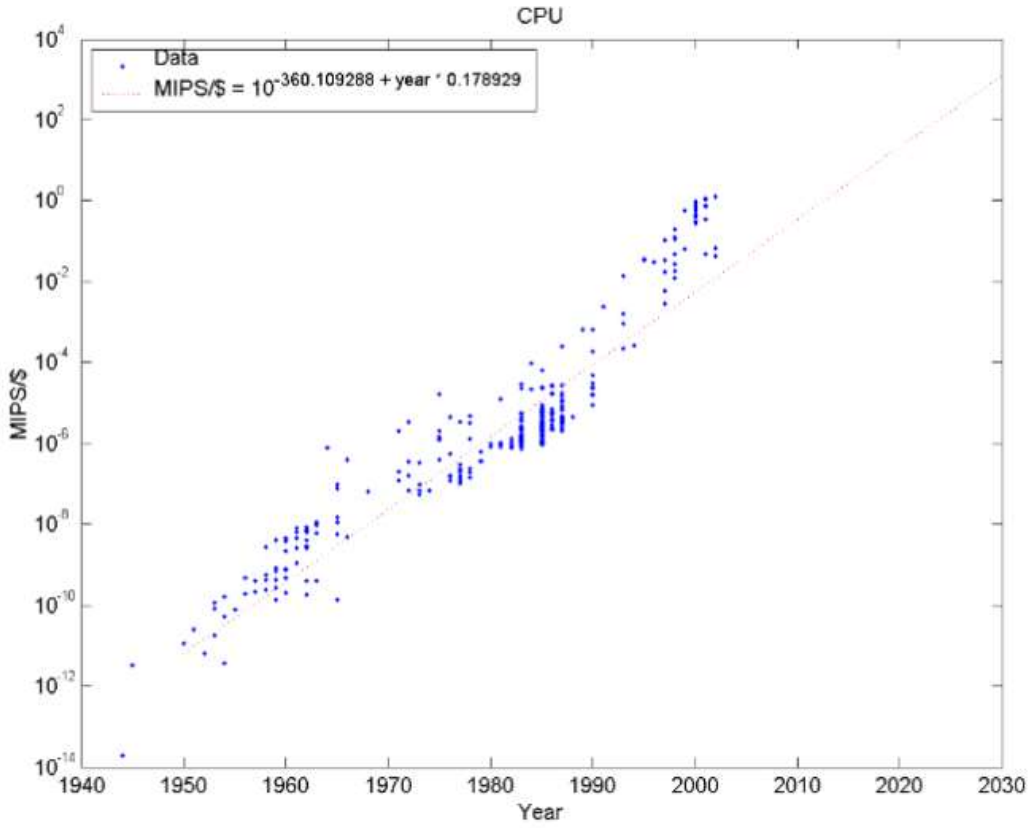

Figure 1. *Processor power in millions of instructions per second per dollar (2007) [51] p. 87*

2.2 Maintenance of Assets

The most rudimentary form of maintenance is reactionary maintenance where components are serviced once a breakage is identified. This is often unacceptable as sudden stops in operations can be very costly [1] and breakages can cause damage to other components down the line. The next step along the road to better maintenance is preventive maintenance. Preventive maintenance is based on the assumption that we can calculate the useful lifetime of the component based on its design parameters and thus plan maintenance intervals. These predictions are often flawed since fatigue of the components is dependent on the operational conditions and predicting these parameters in the design face is often quite challenging. The result of this is that large proportion of breakages can appear random in nature causing components being serviced too early or too late. A United States Navy study in 2001 into its submarine fleet revealed that as much as 71% of component failures appeared random [2].

To combat these gaps in the knowledge, measurement tools are introduced to the system to monitor the operational characteristics and status of the components, such as their vibrational output. The maintenance plan for the asset can be then adjusted according to the component condition. Implementation of a more complex condition based maintenance scheme is often more costly, but these costs can be offset by the savings made in longer maintenance intervals and reduction of unplanned breakages [53].

Setting up a condition monitoring system is not as simple as installing some sensors. The data in and of itself is not necessarily that useful since some failure modes are hard to detect or time from detection to failure might be short. For example bearing roller surface damage is hard to detect as the damaged area and the raceway must be in contact while there is loading on that

specific contact in order for the damage to show in vibrational output [3]. Vibrational signals can be further distorted by other vibration sources in the machine such as hydraulics and motors [52]. To combat these difficulties, the sensor can be mounted closer to the point of interest, but this can pose additional challenges. In the case a of a thruster for example, the thruster pod is a very hostile environment with a wide range of temperature and the sensors being submerged in oil.

To supplement the shortsightedness of a direct condition measurement, a prediction system with a longer horizon can be setup. For predictive maintenance, there are two different paths we can take, a data-based route using machine learning or a system physics model -based route, both with their advantages and disadvantages. The advantages in doing the predictions using machine learning is that the understanding of the underlying physical phenomena doesn't have to be as in depth since the training is done using dataset with linked inputs and outputs [54]. The need for such a comprehensive dataset is also the downside of such a scheme since, this data might not be yet even recorded or not plausible to generate for asset where production numbers might be low. The physics -based approach is the other side of the coin since creation of such a model requires detailed understanding of the system. This is advantageous in cases where asset series are small or with variation between assets such that they are not comparable. Another aspect is the lifetime of the asset, since in such cases collection of the dataset takes a substantial amount of time. Both of these mentioned cases hold true for azimuthing thrusters, so the physics-based approach hold a clear advantage.

2.3 Component Fatigue

Fatigue is often attributed as the most common failure mechanism in machine elements [57] p. 1 [58]. Fatigue can be defined as change in material properties due to stress cycles, with stress levels sometimes well below the tensile strength of the materiel, leading to fractures propagating from microscopic imperfections in the material. Fatigue is also a substantial factor from economic perspective, costing somewhere around 5% of GDP in developed countries [59] [58] see [60]. These costs are due to factor such as increased material needed for construction, inspections, maintenance and others discussed in Chapter 2.1.

Study into fatigue of machine elements and their materials started in the 18-hundreds brought on by the first industrial revolution and the raise of the railway as a means of transportation for both man and material. The beginnings of this new method of transportation was disturbed by serious accidents, most notably the 1842 accident in Versailles France, leading to death of at least 52 people and injury of many more [55] p. 59, 60, resulting from a broken axle in the locomotive [56] p. 1 see [57].

The first studies into fatigue we made by Wilhelm Albert in 1829 when he observed the failure in mine elevator chains due to repeated loading from driving the elevator. Albert was able to establish a connection between loading and fatigue using his constant amplitude test aparatus [58]. Following his tests, perhaps more famously, he invented the wire rope [61]. The wire has the characteristic in that it can withstand damage in form of individual string breaking without the overall structure of the rope being compromised.

Albert Wöhler, one of the best know names in fatigue along with Miner and Palmgren, has many contributions to the field of fatigue springing from his investigations to railway axles. In his earlier work he suggested that axles should be designed in reference to the journal bearings with a finite life taking to consideration the probabilistic nature of these design analyses [61], both of which are important concepts in fatigue design and analysis today. Wöhler also stated that fatigue failure can manifest well below the allowable static stress of the material and that fatigue failure is mostly affected by the amplitude of the loading, but also the mean of this cyclic stress [61]. This combined stress criterion of stress mean and amplitude is sometimes also called the "signed von Mises" stress. Wöhler was also recognized the effect of notches, something already noted by Morin in 1853 [61] see [62], and size as something that decreases the fatigue life of a component [61].

Wöhler noted that the results he had compiled were not directly usable for non-standard shapes as these altered the stress conditions in the components and this is something that standards such as ISO 281 and DIN 743 used in this thesis try to tackle. Perhaps a bit ironically, Wöhler didn't present his stress-cycle data in the form of the curves that bear his name today, but in table form. The logarithmic form of Wöhler curve we know today was introduced much later in 1910 by Basquin [61] see [63].

The fatigue damage accumulation equation, presented in Chapter 3.1.4, was first introduced by Palmgren [61] see [64]. The rule was discussed a lot by Langer, Thum, Kommers and Miner, who finally popularized it in 1945 [26][61], but interestingly Miner didn't reference Palmgrens original paper. Palmgren was also responsible for the first statistical approach into component design [61] with his definition of ball bearing life [9] which serves as the base for the ISO 281 standard.

After the World Wars the raise of the aerospace industry, and subsequent crashes such as the two Comet incidents in 1954 [56] p. 4, was the main driver in fatigue research. The failure in the one piece hull of the Comet led to an unstoppable fracture propagation [61], somewhat similarly as with the welded hulls of the Liberty ships. These crashes led to definition of more extensive fatigue testing of the airframes and pre-flight inspection with scheduled maintenances where components would be replaced before end of life [61].

3. BEARING MODEL

In this chapter we look over the theory for different levels of complexity starting with the basic rating life calculation method pioneered by Lundberg and Palmgren, and its evolution to the reference bearing life calculation. To include the effects of the operating conditions these calculation methods can be modified with the use of a modification factor calculated as a function of viscosity and contamination. In our scope contamination means introduction of particles into the lubricant. Other contaminants such as water in the lubricant also hinder the fatigue performance of bearings, but its effects were left outside of this work. Quantification of contamination is further discussed in 3.1.2. In the end we will have a brief description of the function of the calculation program written in Python 3.

Rolling bearings can exhibit several different failure modes based on their environment, operating conditions and loading profiles. International standard ISO 15243 divides the bearing failure modes into 6 main categories based on their primary cause:

1. fatigue
2. wear
3. corrosion
4. electrical erosion
5. plastic deformation
6. fracture and cracking [4] p. 2.

Differentiation between failure modes is often very challenging as they are interconnected. For example contact fatigue, which is the scope of this thesis, can cause flaking, pitting and peeling in the contacting bodies [5] p. 177 [4] p. 3 releasing particles into the lubricant. These particles can cause wear in the bearing itself or in other components down the lubrication line, if sufficient filtration is not implemented.

The fatigue in the bearing elements is caused by the cyclic loading of rolling elements as they rotate in and out of loaded positions. Even though the bearing itself might be statically loaded, the bearing components experience cyclic loading. The applied loading on the contact between the rolling element and the bearing ring raceway creates high Hertzian pressures that are typically around 1500 MPa but can go as high as 3500 MPa [5] p. 47 [6] p. 102. Even though the pressures can be quite high the affected area remains small in terms of the volume of the rolling element and thus the fatigue damage is limited to the rolling surfaces [6] p. 102.

Bearing fatigue life calculations presented in international standards ISO 281:2007 and ISO 16281:2008 are based on the surface and subsurface fatigue caused by Hertzian pressures in the contact. These standards were chosen for the bearing fatigue module application as they are well recognized methods and thus it is easier to communicate the new technology to the classification societies and customers. In addition to the bearing loading, these standards also take into consideration the bearing clearance, roller profiles, raceway profiles, lubrication and contamination.

3.1 Theory

3.1.1 Basic Rating Life

ISO 281 defines the bearing life as a number of revolutions the bearing can endure before any of the loaded components of the bearing, i.e. bearing rings and rolling elements, exhibit fatigue damage [8] p. 2. This means that even though the bearing has not suffered a critical failure and can remain operational, the operational requirements regarding noise, vibration and load bearing capacity for example, are no longer met. When the bearing is at the end of its life, it is prudent to replace the faulty bearing as the continued operation can cause damage to other components, for example cause by the increased vibration and contaminating particles from flaking of contact surfaces.

Bearing fatigue calculation presented in the ISO 281 standard is based on the model presented by Lundberg and Palmgren in their 1947 and 1952 papers. They based their life calculation model on the research made by Weibull [11] [12] into the probabilistic nature of failure in materials.

Unlike Weibull, who assumed that crack formulation will necessarily lead to damage on the surface, Lundberg and Palmgren found out that not all cracks will reach the surface and thus cause damage to the contact surfaces [9], p. 13. Based on the knowledge that the probability of breakage is dependent on the depth, they introduced parameter z_0, which is the depth of the most critical shear stress τ_0, to the life formula. Thus the life equation was written as

$$\log\frac{1}{S} \approx \frac{\tau_0^c N^e a l}{z_0^{h-1}}, \tag{1}$$

where S is the probability of survival, N is the number of cycles in million cycles, a is the semi major width of the Hertzian contact and l is the length of raceway in the direction of the contact major diameter [9] p. 13. Exponents c, e and h are determined via experiments [9] p. 15, of which e is called life scatter factor [14] p. 4. Lundberg and Palmgren further defined equation (1) based on Hertz's theory of contact into

$$L_{10} = \left(\frac{C}{P}\right)^p, \tag{2}$$

where C is basic dynamic load rating, P is the dynamic equivalent load, p is the load life exponent and L_{10} is the bearing life in millions of cycles with a 90% probability of survival [9] p. 15. This is the life equation presented in the ISO 281 international standard and today it is known as the basic or catalog rating life [8].

Rolling bearings can be divided into two main categories: ball bearings and roller bearings. For ball bearings, which experience point contact, the value of $p = 3$ was determined by Lundberg and Palmgren based on fatigue test experiment on 270 ball bearings [9] p. 17. Determination of the exponent for roller bearings is more challenging since construction of roller bearings that experience uniform pressure distribution with a wide loading spectrum is not feasible [9] p. 18. Rollers are usually crowned in effort to alleviate edge loading in heavy load conditions [6] p. 127. Depending on the degree of loading and thus the profile of the roller, it can experience point or line contact and even a combination of them [6] p. 128 [9] p. 19. For bearings and loading conditions where a pure line contact exists between both inner ring and outer ring contacts, the value of the exponent was determined at $p = 4$ [9][10] p. 6. This however doesn't adequately reflect the real world operating conditions where high loads cause the contact to transform closer to a line contact and with lower loads the contact more closely resembles a point contact [10] p. 11. Based on the knowledge that the exponent should lie somewhere between 3 and 4, Lundberg and Palmgren determined $p = 10/3$ to be appropriate for roller bearings [10] p. 13. Values of $p = 3$ for ball bearings and $p = 10/3$ for roller bearings were also adopted to ISO 281 standard [8] p. 10, p. 16.

Basic dynamic load rating is a theoretical centric constant loading in the primary bearing loading direction, radial load for radial bearings (subscript r) and axial load for thrust bearing (subscript a), that the bearing can withstand achieving a basic rating life of one million revolutions or $L_{10} = 1$ [9] p. 24 [8] p. 2. ISO 281 presents formulas for the calculation of basic dynamic load rating for each of the four bearing classes. For radial ball bearings

$$C_r = b_m f_c (i * \cos(\alpha_0))^{0.7} Z^{2/3} D_w^{1.8}, \text{when } D_w \leq 25.4 \text{ mm}, \tag{3}$$

$$C_r = 3.647 b_m f_c (i * \cos(\alpha_0))^{0.7} Z^{2/3} D_w^{1.4}, \text{when } D_w > 25.4 \text{ mm} \tag{4}$$

and for thrust ball bearings

$$C_a = b_m f_c Z^{2/3} D_w^{1.8}, \text{when } D_w \leq 25.4 \text{ mm and } \alpha_0 = 90°, \tag{5}$$

$$C_a = b_m f_c (\cos(\alpha_0))^{0.7} \tan(\alpha_0)\, Z^{2/3} D_w^{1.8}, \text{when } D_w \leq 25.4 \text{ mm and } \alpha_0 \neq 90°, \tag{6}$$

$$C_a = b_m f_c Z^{2/3} D_w^{1.4}, \text{when } D_w > 25.4 \text{ mm and } \alpha_0 = 90°, \tag{7}$$

$$C_a = 3.647 b_m f_c (\cos(\alpha_0))^{0.7} \tan(\alpha_0)\, Z^{2/3} D_w^{1.4}, \text{when } D_w > 25.4 \text{ mm and } \alpha \neq 90° \tag{8}$$

[8] p. 6, 10. For radial roller bearings

$$C_r = b_m f_c (i L_{we} \cos(\alpha_0))^{7/9} Z^{3/4} D_{we}^{29/27} \tag{9}$$

and for thrust roller bearings

$$C_a = b_m f_c L_{we}^{7/9} Z^{3/4} D_{we}^{29/27}, \text{when } \alpha_0 = 90°, \tag{10}$$

$$C_a = b_m f_c (L_{we} \cos(\alpha_0))^{7/9} \tan(\alpha_0)\, Z^{3/4} D_{we}^{29/27}, \text{when } \alpha_0 \neq 90° \tag{11}$$

[8] p. 13, 17. In equations (3) to (11) b_m is the rating factor, f_c is the geometrical factor, i is the number of rows in the bearing, α_0 is the nominal contact angle, Z is the number of rolling elements per row, L_{we} is the effective roller length in millimeters, D_w is the ball diameter in millimeters and D_{we} is roller diameter in millimeters. Subscript *a* refers to axial or thrust bearings, subscript *r* to radial bearings, subscript *w* to ball bearings and subscript *we* to roller bearings. Values for the rating factor b_m for thrust ball bearings is b_m = 1.3 [8] p. 10 and the rest of the values can be determined from reference [8] tables 1, 6 and 9. Values for the geometrical factor f_c can be determined from reference [8] tables 2, 4, 7 and 10. The values vary roughly from 10 to 200 depending on type and dimensions.

The method for calculating bearing basic dynamic capacity presented in ISO 281 is based the methodology presented in reference [9] p. 32. However these formulas presented by Lundberg and Palmgren were deduced for bearings manufactured with materials and production techniques available in the 1940s and 1950s [6] p. 215. With modern materials and production techniques, such as vacuum melted steels, we can produce bearings with better fatigue properties and thus there is an increase in the basic dynamic capacity over time [6] p. 238. Thus the formulas have been adjusted to the form above to fit the make of the bearings correctly. The current ISO standard assumes the bearings are made of 52100 high carbon chrome steel and hardened to a minimum of 58 Rockwell hardness [6] p. 238 [13].

Dynamic equivalent load P is a sum of forces acting on the bearing formulated in such a way that it represents the real loading condition [9] p. 36. The formulation differs between bearing types and primary loading directions. For bearings with nominal contact angle and loading parallel to the main loading direction of the bearing the dynamic equivalent load equals to the applied loading such that

$$P_r = F_r, \text{when } \alpha_0 = 0 \tag{12}$$

for radial bearings and

$$P_a = F_a, \text{when } \alpha_0 = 90° \tag{13}$$

for axial bearings [8] p. 8, 12, 15, 19. F_r is the radial loading component and F_a is the axial loading component. However, when both loading components are present or the nominal contact direction doesn't coincide with main loading direction, it has to be taken to be taken into account according to

$$P = XF_r + YF_a \tag{14}$$

where X is the radial loading factor and Y is the axial loading factor [8] p. 9, 12, 15, 19. The original formulation from [9] p. 42, 44 also included a rotational factor in the radial loading term but it was excluded from the 2007 release of ISO 281. This was due to the low variation of the value of the variable [14] p. 17. Appropriate values for loading factors can be found from reference [8] tables 3, 5, 8 and 11. When choosing appropriate values for a bearing and loading condition one compares the ratio of axial load and radial load to the life scatter exponent e. The table values are calculated based on load integrals and a thorough formulation for these values can be found in [9] [10] [14].

3.1.2 Modified Bearing Life

Lundberg-Palmgren model assumes the fatigue is initiated in a subsurface level from slag or other inclusions in the steel [18] p. 368. Advancements in the field of manufacturing have led to better and cleaner resulting in surface stress becoming more prevalent [17] p. 6. This means fatigue damage in modern bearings is more often surface initiated than subsurface initiated. additionally, the effects of lubrication and thus the presence of an oil film between the contact pairs are also overlooked by Lundberg and Palmgren due to the lack of knowledge at the time [18] p. 367. They idealized the contact so that only normal forces are transmitted according to the Hertzian theory [9] p. 5, which is only the case for undamaged ideal geometries [17] p. 19. Lastly, the Lundberg-Palmgren model predicted all bearing lives to be finite in nature since the idea of a bearing fatigue limit was not yet established [18] p. 367.

In an effort to account for differences in bearing construction and operation, the 1987 revision of ISO 281 introduced three independent factors to the Lundberg-Palmgren life model; reliability factor, bearing construction factor and operating factor [15] p. 36. Reliability factor was to account for different levels of reliability based on a Weibull distribution [14] p. 5, the second one was determined by the manufacturer based on the bearing construction and materials and the last one was based on operating and mounting conditions such as lubrication [15] p. 36.

Reliability factor a_1 was correctly formulated as an independent factor as it is calculated based on the desired reliability S on the Weibull distribution of bearing lives [15] p. 36 [14] p. 3. Reliability describes share of bearings from a random sampling that achieve the calculated life. Different calculation schemes for reliabilities above and below 90 % are introduced to more accurately represent the increased load capacity, resulting from tapering, at higher reliability percentages. Reliability factor for ranges $S \geq 90$ % is calculated with a three parameter Weibull distribution reduced to [14] p. 5

$$a_1 = 0.95\left[\frac{\ln\left(\frac{100}{S}\right)}{\ln\left(\frac{100}{90}\right)}\right]^{2/3} + 0.05 \tag{15}$$

It should be noted that when reliability is 90 %, reliability factor is 1, which is the default value for bearing life calculation.

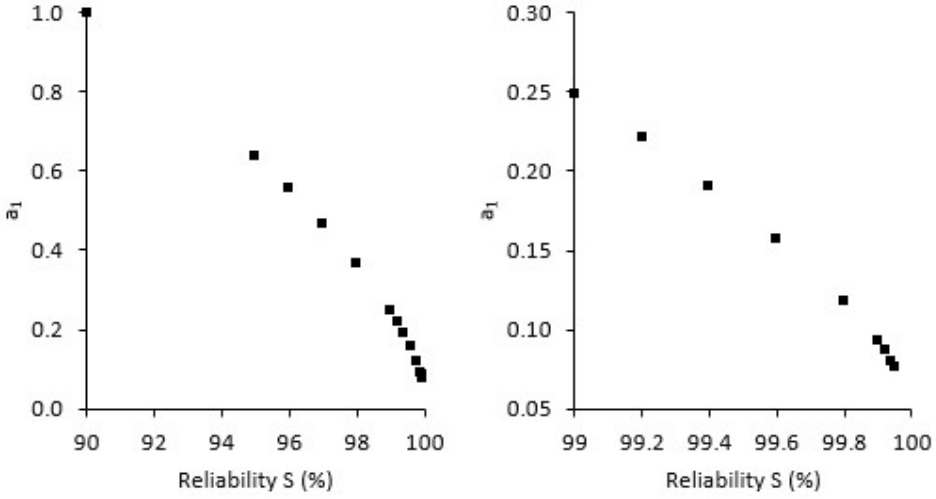

Figure 2. *Visualisation of the reliability factor a_1 for $S \geq 90$ %*

For reliabilities below 90 %, reliability factor is calculated with [14] p. 3

$$a_1 = \left[\frac{\ln\left(\frac{100}{S}\right)}{\ln\left(\frac{100}{90}\right)}\right]^{1/e}, e = 1.16, \tag{16}$$

where the exponent e was calculated by trying to match the results to [6] p. 203 figure 11.8 as no concrete values were not provided in the standard nor the technical specification.

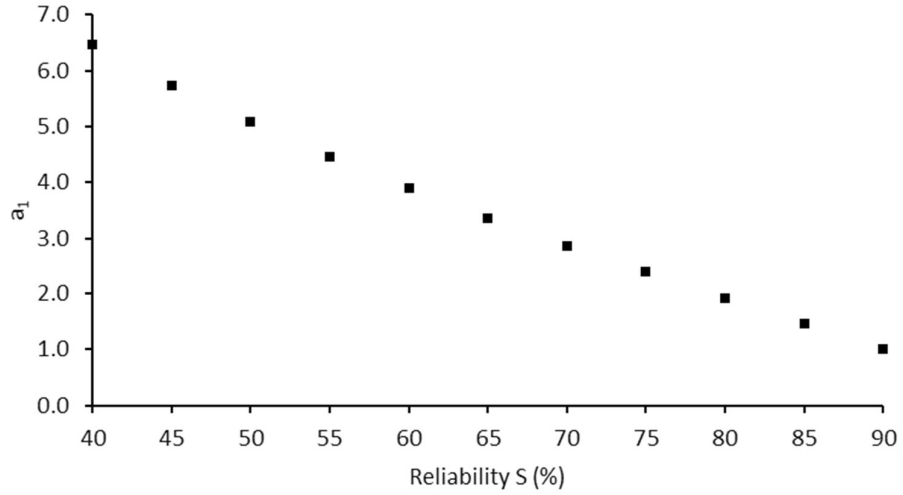

Figure 3. *Visualisation of the reliability factor a_1 for S < 90 %*

The exponent should be in the range of 1 to 1.5 [19] or for more modern steel in the range of 0.7 to 3.5 [6] p. 208. Exponent of 1.16 should be then adequately conservative as lower values present lesser quality of the bearing and thus higher dispersion [6] p. 208. From Figure 2 and Figure 3 we can see that the reliability factor doesn't behave linearly, since bearings fatigue lives follow a Weibull distribution, but trends downwards with higher reliability values and upwards when lover values. If exponent *e* were larger, the slope would be much steeper.

In time bearing manufacturers recognized that the two factors of bearing construction and operating conditions were interdependent rather than independent. So, the manufactures started combining these to a single factor. Calculation models for these factors were not standardized so seemingly identical bearings in identical conditions had widely different fatigue life depending on the manufacturer [15] pp. 36-39.

The first step towards the life modification factor a_{ISO} was presented by Ioannides and Harris in 1985 who introduced the bearing fatigue limit σ_u along with their updated bearing fatigue life model [17]

$$\ln\frac{1}{S} \approx AN^e \int_{V_{risk}} \frac{\langle \tau - \tau_u \rangle^c}{z'^h} dV, \tag{17}$$

where *A* is the proportionality scaling factor, *V* represents volume, τ is the combined stress (e.g. von Mises stress) and *z'* is stress-weighted depth. This function is constructed with the assumption, if stress remains under the fatigue limit, no damage is cumulated. Fatigue limit for bearings is generally reached when contact pressure reaches 1500 MPa [8] p. 21. When comparing Equation (1) to Equation (17), one can notice some similarities [18] p. 371. This formulation however lacked the simplicity of the basic rating life calculation of Equation (2). In an effort to adapt use of the fatigue limit to the basic rating life formula Ioannides et al. [17] pp. 24-30 formulated the a_{SLF} (stress life factor) which was adopted in the ISO 281:2007 as a_{ISO}.

In Equation (1) we can substitute the most critical shear stress amplitude τ_0 with the value of stress above fatigue limit τ_u such that

$$\ln\frac{1}{S} \approx N^e \frac{\langle \tau_0 - \tau_u \rangle^c}{z_0^h} a z_0 l, \tag{18}$$

or alternatively

$$\ln\frac{1}{S} \approx \frac{N^e \tau_0^c a z_0 l}{z_0^{h-1}} \langle 1 - \frac{\tau_u}{\tau_0} \rangle^c, \tag{19}$$

such that left side of the equation is the basic rating life equation and the right side is the fatigue term [17] p. 9, 10. Working the Equation (19) along [9] pp. 13-15 and [17] pp. 10-12 we can solve the equation in terms of bearing life L_{10} as

$$L_{10} = A\frac{1}{\langle 1 - \left(\frac{C_u}{P}\right)^w \rangle^{c/e}}\left(\frac{C}{P}\right)^p, \tag{20}$$

where C_u is the fatigue load limit of the bearing and w is a load life exponent. Load life exponent is defined identically to how P. Ioannides et at. determined values of w = 1/3 for point contacts and w = 1/2 for line contacts [17] p. 12. Fatigue load limit is the amount of loading that causes the stress in the most loaded roller raceway contact to reach the fatigue limit of the material [8] p. 3. In ISO 281 the value of the proportionality scaling factor A, which is the asymptote of the heaviside function as dynamic equivalent load P → ∞, is set to A = 0.1 as the result of extensive testing [16] p. 20, 46, 47.

This formulation of the bearing life takes into account the fatigue limit of the bearing, but still neglects the effects of lubrication, contamination of lubricant and surface quality, all of which can affect the stress concentrations in the contact [17] p. 19. To take these factors into consideration, we introduce a life factor η to Equation (20) such that [17] p. 20

$$L_{10} = A\frac{1}{\langle 1 - \left(\eta\frac{C_u}{P}\right)^w \rangle^{c/e}}\left(\frac{C}{P}\right)^p, 0 \le \eta \le 1. \tag{21}$$

Life factor η can be further broken down to components such that

$$\eta = \eta_a\eta_b\eta_c. \tag{22}$$

Macro stress factor η_a is related to stresses resulting from mounting, centrifugal forces and residual stresses from manufacturing. In the case of ISO 281, these effects are considered to be insignificant, so we can set η_a = 1 [17] p. 25. The latter two micro scale components [17] pp. 60-62 are lubrication factor η_b and contamination factor η_c, which is marked with e_C in the ISO 281 standard [14] p. 7. Macro level stresses affect the deeper material levels and micro level stresses the surface and near-surface material layers [17] p. 60. These factors can be considered independently as they contribute to different failure modes. Lubrication affects the surface shear stresses as the surface asperities come into contact if lubrication is lacking. Particle contaminants in the lubricant cause dents to the contacts surfaces that create stress concentrations causing spikes in the orthogonal shear stress near the surface [17] p. 62. From Equations (21) and (22), A = 0,1 and η_a = 1 we can denote the life modification factor as

$$a_{ISO} = 0.1\langle 1 - \left(\eta_b\eta_c\frac{C_u}{P}\right)^w \rangle^{-c/e}. \tag{23}$$

Lubrication factor is determined by comparing the relation of the life modification factor of an actual bearing and an ideal bearing with ideal lubrication conditions. The results for η_b are plotted as a function of viscosity ratio κ in [14] p. 8 Figure 4. From these results general form for lubrication factor is derived as

$$\eta_b = \Psi_{brg}\left(3.387 - \frac{b_0}{k^m}\right)^{5/2}, \tag{24}$$

where ψ_{brg} is a characteristic factor for the type of bearing, e. g. radial ball bearing (rbb), radial roller bearing (rrb), thrust ball bearing (trb) or thrust roller bearing (trb). Factors b_0 and m are factors specific for different viscosity ratio ranges [14] p. 8.

Viscosity ratio is the relation of operational dynamic viscosity and reference dynamic viscosity

$$\kappa = \frac{v}{v_1}, 0.1 \le \kappa \le 4, \tag{25}$$

where v is the operational viscosity and v_1 is the reference viscosity [8] p. 25. Reference viscosity is the minimum required viscosity required to separate the contacting bodies to avoid metal-to-metal contacts [8] p. 25. The range of viscosity ratio is restricted for at the lower end calculation model is not currently verified and at the higher end any increase provides diminishing returns in terms of better fatigue endurance [8] p. 27. In ISO 281 bearing contacts are assumed to have good surface quality [8] p. 1, so the calculation for reference viscosity is rather simple only including the pitch diameter of the bearing and operational speed such that

$$v_1 = 45000n^{-0.83}D_{pw}^{-0.5}, \text{when } n < 1000 \text{ rpm} \tag{26}$$

$$v_1 = 45000n^{-0.5}D_{pw}^{-0.5}, \text{when } n \geq 1000 \text{ rpm} \tag{27}$$

A higher viscosity is required for higher operational speeds as centrifugal forces caused by the rotation can force the lubricant away from the contact region [15] p. 39.

Contamination factor is determined in the same manner as the lubrication factor by comparing the life modification factor of a dented contact with an ideal [14] pp. 10-13 [17]. p. 74, 75. For use in ISO 281, a simplified version of the model depending on bearing pitch diameter, relative viscosity and ISO 4406 oil cleanliness was adopted [14] p. 13. Contamination factor is calculated with

$$e_C = a\left(1 - \frac{c_1}{D_{pw}^{1/3}}\right), \text{where } a = c_2\kappa^{0.68}D_{pw}^{0.55}, \text{with restriction } a \leq 1 \tag{28}$$

where c_1 and c_2 are constants depending on the lubrication system and cleanliness [8] pp. 34-42.

Table 1. *Constants for systems with in-line filtration [8] p. 34, 35*

ISO 4406 cleanliness	-/13/10, -/12/10, -/13/11, -/14/11	-/15/21, -/16/12, -/15/13, -/16/13	-/17/14, -/18/14, -/18/15, -/19/15	-/19/16, -/20/17, -/21/18, -/22/18
c_1	0.5663	0.9987	1.6329	2.3362
c_2	0.0864	0.0432	0.0288	0.0216

Table 2. *Constants for systems without filtration or with off-line filters [8] pp. 36-38*

ISO 4406 cleanliness	-/13/10, -/12/10, -/11/9, -/12/9	-/15/12, -/14/12, -/16/12, -/16/13	-/17/14, -/18/14, -/18/15, -/19/15	-/19/16, -/18/16, -/20/17, -/21/17	-/21/18, -/21/19, -/22/19, -/23/19
c_1	0.6796	1.141	1.67	2.5164	3.8974
c_2	0.0864	0.0288	0.0133	0.00864	0.00411

Table 3. *Constants for systems with grease lubrication [8] pp. 39-41*

ISO 4406 cleanliness	High cleanliness	Normal cleanliness	Slight to typical contamination	Severe contamination	Very severe contamination
c_1	0.6796	1.141	1.887, when $D_{pw} < 500$ mm 1.677, when $D_{pw} \geq 500$ mm	2.662	4.06
c_2	0.0864	0.0432	0.0177	0.0155	0.00617

Values for constants in Equation (28) can be found from Table 1, Table 2 and Table 3 respectively. ISO 4406 codes from left to right in the aforementioned tables tells us the maximum number of particles larger than 4 µm, 6 µm and 14 µm. The actual particle counts are calculated as powers of two, such as $2^{\text{ISO4406\_code}}$ / 100 [20]. To clarify this with and example, ISO 4406 code 12/14/17 tells us that there are between 2^{11} and 2^{12} 4 µm particles, between 2^{13} and 2^{14} 6 µm particles and between 2^{16} and 2^{17} 14 µm particles.

Now we can substitute η_b in Equation (23) with Equation (24) and η_b with e_C such that

$$a_{ISO} = 0.1\left\langle 1 - \left(\Psi_{brg}\left[3.387 - \frac{b_0}{k^m}\right]^{5/2} e_C\frac{C_u}{P}\right)^w \right\rangle^{-c/e}, \tag{29}$$

from which we can get to the ISO 281 formulation of the bearing life modification factor [8] pp. 27-31

$$a_{ISO} = 0.1\left[1 - \left(\Psi_{brg} - \frac{b_0}{k^m}\right)^{2.5w}\left(\frac{e_C C_u}{b_1 P}\right)^w\right]^{-c/e}, \text{with restriction } a_{ISO} \leq 50, \tag{30}$$

where b_1 is a factor for equivalent dynamic loading. It should be noted that this formulation differentiates from the formulation presented in [17] pp. 25-27 due to differences in the way fluctuations in the contact stress profile caused by contaminants are handled [15] p. 26. From Figure 4 we can clearly see the effects of the life modification factor for radial roller bearings with different lubrication and load-contamination conditions. Additionally, there is an increase in life as lubrication condition improve towards the 1, but after that the increase starts to diminish as described above. With extremely heavy load-contamination better lubrication provides little help but if the load is only medium to heavy, proper lubrication provides substantial benefits. It should also be noted that if lubrication is severely lacking, decreasing load-contamination provides little help. Life modification factor is capped to 50 due to practical considerations [8] p. 27.

Table 4. *Values for bearing life modification factor for radial bearings*

	Radial ball bearing			Radial roller bearing		
	$0.1 \le \kappa < 0.4$	$0.4 \le \kappa < 1$	$1 \le \kappa < 4$	$0.1 \le \kappa < 0.4$	$0.4 \le \kappa < 1$	$1 \le \kappa < 4$
Ψ_{brg}	2.5671	2.5671	2.5671	1.5859	1.5859	1.5859
b_o	2.2649	1.9987	1.9987	1.3993	1.2348	1.2348
b_1	1	1	1	1	1	1
m	0.054381	0.19087	0.071739	0.054381	0.19087	0.071739
w	1/2.5	1/2.5	1/2.5	1/2.5	1/2.5	1/2.5
-c/e	-9.185	-9.185	-9.185	-9.185	-9.185	-9.185

Table 5. *Values for bearing life modification factor for thrust bearings*

	Thrust ball bearing			Thrust roller bearing		
	$0.1 \le \kappa < 0.4$	$0.4 \le \kappa < 1$	$1 \le \kappa < 4$	$0.1 \le \kappa < 0.4$	$0.4 \le \kappa < 1$	$1 \le \kappa < 4$
Ψ_{brg}	2.5671	2.5671	2.5671	1.5859	1.5859	1.5859
b_o	2.2649	1.9987	1.9987	1.3993	1.2348	1.2348
b_1	3	3	3	2.5	2.5	2.5
m	0.054381	0.19087	0.071739	0.054381	0.19087	0.071739
w	1/3	1/3	1/3	1/2.5	1/2.5	1/2.5
-c/e	-9.3	-9.3	-9.3	-9.185	-9.185	-9.185

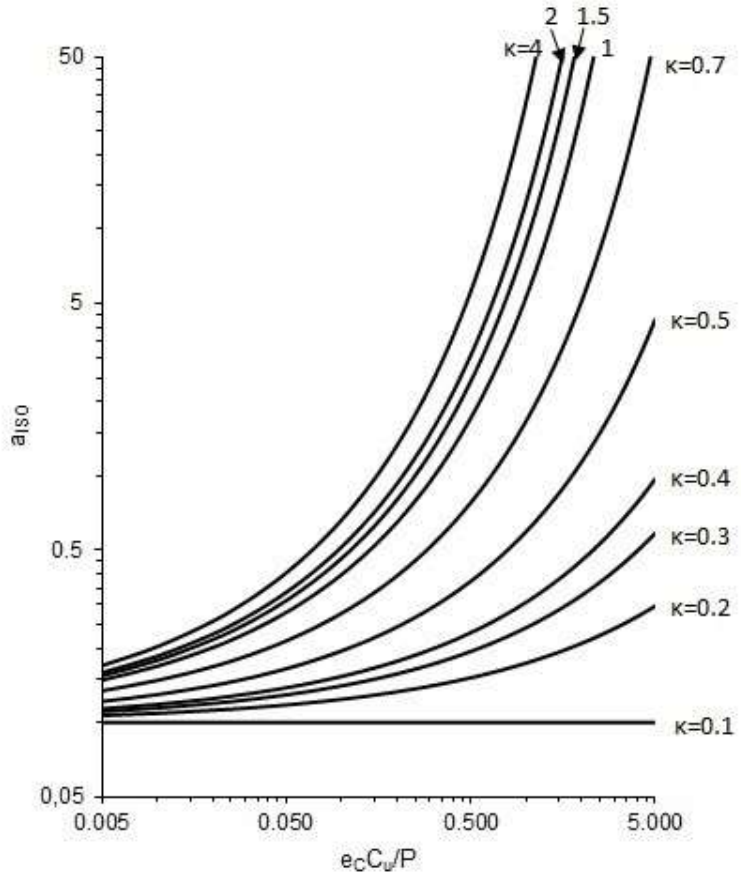

Figure 4. *Bearing life modification factor for radial roller bearings*

Values for Equation (30) for relevant bearing type and lubrication conditions can be found in Table 4 and Table 5. Combining Equations (2), (30) and (15) or (16) depending on the required reliability level we can write the modified basic bearing life equation such that [8] p. 20

$$L_{nm} = a_1 a_{ISO} L_{10} \tag{31}$$

Subscript *n* is marks the reliability in the same vein as with basic rating life notation e. i. *n* = 100 - *S.* Subscript *m* stands for modified.

3.1.3 Reference Rating Life

One of the short comings of basic bearing life model is its inability to accurately predict the bearing fatigue life when the bearing is subjected to higher loads. Higher loads can cause plastic deformations of the bearing components and edge loading resulting in spikes in the contact pressures at the rolling element ends [6] p. 127-129. The breaking point for the model is roughly when dynamic equivalent load reaches half of the basic dynamic load rating [8] p. 10, 13, 16, 20. Another factor is the installation of the bearing in terms of tilting and clearance [21] p. 1. Clearance affect the internal load distribution of the bearing and tiling the shape of the pressure distribution in the roller-raceway contact. In the scope of this work we make the following assumptions:

1. Effects of tiling are ignored for shafts in thrusters being very stiff [7] p. 3 due to marine regulations
2. Bearings are either radially or axially loaded
3. Rollers are loaded symmetrically
4. With multirow bearings, the load is assumed to be distributed evenly on all rows
5. Outer ring is assumed to be stationary and inner ring to rotate

For radial bearings the degree of loaded rolling elements [6] p. 138

$$\varepsilon = \frac{1}{2}\left(1 - \frac{P_d}{2\delta_r}\right) \tag{32}$$

depends on diameter clearance P_d and radial ring shift δ_r. Diameter clearance is the amount of linear radial movement in the bearing when one of the rings is fixed and the other is moved up and down or side to side. Radial ring shift is the amount of radial movement caused be the loading from a position when both bearing rings are concentric.

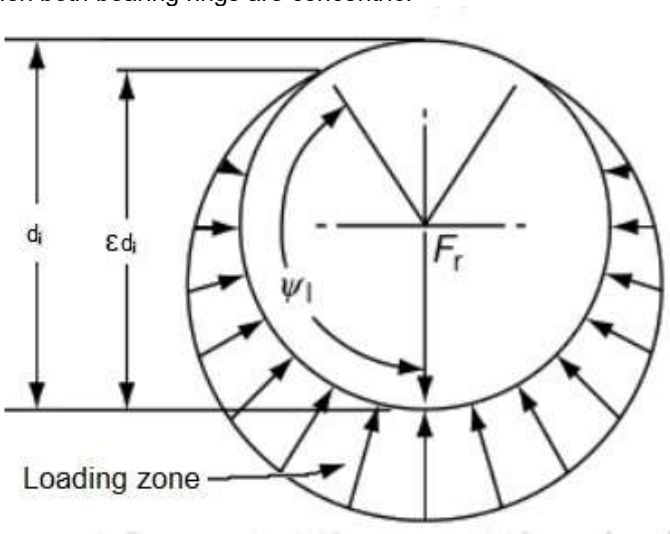

Figure 5. *Loading zone of inner ring, created from [6] p. 141*

From Equation (32) we can also get the extent of the loading zone in terms of the angular limit for the loading zone such that [6] p. 138

$$\psi_l = \cos^{-1}\left(\frac{P_d}{2\delta_r}\right) \tag{33}$$

When radial clearance is positive, $\varepsilon < 0.5$ and $\psi_l < 90°$. If bearing has zero radial clearance, exactly half of the bearing ring is loaded. In preloaded bearings, meaning diameter clearance is negative, loading zone extends to over half of the bearing ring [6] p. 141, such as in Figure 5, where d_i is the diameter of inner raceway.

General form for roller element load is

$$Q = K\delta^k \tag{34}$$

where K is combined stiffness, δ is contact deformation and k is contacts specific exponent. For point contacts $k = 3/2$ and for line contacts $k = 10/9$ [6] p. 137. When we calculate the load distribution for the rolling elements, we assume the loading to be equal in both inner ring and outer ring contacts. Deformations are also summed together to simplify the calculation and individual deformations can be solved later if needed. Combined stiffness can be calculated from inner ring contact stiffness K_i and outer ring contacts stiffness K_o such that

$$K_t = \left[\left(\frac{1}{K_i}\right)^{1/k} + \left(\frac{1}{K_o}\right)^{1/k}\right]^{-k} \tag{35}$$

For line contact stiffness can be calculated such that

$$K = 8.06 \cdot 10^4 L_{we}^{8/9} \tag{36}$$

and for point contacts

$$K = 2.15 \cdot 10^5 \sum\rho^{-0.5}(\delta^*)^{-1.5} \tag{37}$$

where $\sum\rho$ is curvature sum and δ^* is dimensionless deformation [6] p. 137. Curvature sum for contact of two bodies defined by radii in perpendicular directions can be calculated such that

$$\rho = \frac{1}{r} \tag{38}$$

$$\sum\rho = \rho_{11} + \rho_{12} + \rho_{21} + \rho_{22} \tag{39}$$

where r is the radius of the surface and first number in the subscript refers to the body and the second to the direction. Convex radii are positive and convex radiuses are negative. To solve dimensionless deformation we first need to solve curvature difference of the contacting bodies such that [6] p. 51

$$F_\rho = \frac{(\rho_{11} - \rho_{12}) + (\rho_{21} - \rho_{22})}{\sum\rho} \tag{40}$$

From there on we can solve dimensionless deformation based on [6] p. 111 Table 6.1. Any in between values are solved through linear interpolation. Now if we assume that the most critically loaded rolling element is positioned directly along the loading at ψ = 0°, we can calculate the rolling element deformation at that point such that [6] p. 137

$$\delta_{max} = \delta_r - 0.5P_d \tag{41}$$

Once we know the deformation in bottom most rolling element, we can calculate the loading Q_{max} in that position with Equation (34). To calculate other loaded rolling elements we need to figure out the angle between rolling elements based on the knowledge of how many rolling elements there are per row, which are evenly spaced, and the limit of the loading zone from Equation (33). In order to check for load equilibrium, we need to solve the loading for the rest of the loaded rolling elements for their angular positions ψ such that [6] p. 138

$$Q_\psi = Q_{max}\left[1 - \frac{1}{2\varepsilon}(1 - \cos\psi)\right]^k \tag{42}$$

For the system to be in equilibrium, the sum of the rolling element load components in the loading direction must equal to the bearing load such that [6] p. 139

$$F_r = \sum_{\psi=0}^{\psi=\pm\psi_l} Q_\psi \cos\psi \tag{43}$$

where zero angle position is along the axis of radial load F_r. The system can be now solved by iteratively increasing radial ring shift until a stopping condition in reach or with some 2-dimensional optimization algorithm such as the golden-section search [22].

For thrust bearings with centric loading, the load is distributed equally on all rolling elements and the load on a rolling element can be calculated such that

$$Q = \frac{F_a}{Z\sin\alpha} \tag{44}$$

where α is the operational contact angle [6] p. 141. Contact deformations can be solved in the same fashion as with radial bearings, based on loads and stiffnesses.

Let us first consider reference rating life calculations for ball bearings. To do this, we need to determine rolling element load equivalent to the basic dynamic load rating of the bearing. This equivalent load can be calculated such that [21] p. 7, 8

$$Q_c = \frac{C}{b_2}\left(1 + \left\{b_3\left(\frac{1-\gamma}{1+\gamma}\right)^{1.72}\left[\frac{r_i}{r_o}\left(\frac{2r_o - D_w}{2r_i - D_w}\right)\right]^{0.41}\right\}^{c_1}\right)^{3/10} \tag{45}$$

where r_i is the inner ring raceway radius and r_o is the outer ring raceway radius. Constants b_2, b_3 and exponent c_1 can be found from Table 6.

Table 6. *Values for basic dynamic load rating equivalent load calculation for ball bearings*

		b_2	b_3	c_1
Inner ring (Q_{ci})	rrb	$0.407Z\cos(\alpha)i^{0.7}$	1.044	10/3
	trb, $\alpha \neq 90°$	$Z\sin(\alpha)$	1	10/3
	trb, $\alpha = 90°$	Z	1	10/3
Outer ring (Q_{ce})	rrb	$0.389Z\cos(\alpha)i^{0.7}$	1.044	-10/3
	trb, $\alpha \neq 90°$	$Z\sin(\alpha)$	1	-10/3
	trb, $\alpha = 90°$	Z	1	-10/3

Auxiliary parameter γ can be calculated such that [21] p. 3

$$\gamma = \frac{D_w \cos\alpha}{D_{pw}}, \text{for rrb and trb}$$
$$\gamma = \frac{D_{we} \cos\alpha}{D_{pw}}, \text{for rrb and trb} \tag{46}$$

Now we need to calculate the equivalent dynamic rolling element load based on rolling element loads such that [21] p. 8

$$Q_{ei} = \left(\frac{1}{Z}\sum_{j=1}^{Z} Q_j\right)^{1/3} \tag{47}$$

for inner ring and

$$Q_{eo} = \left(\frac{1}{Z}\sum_{j=1}^{Z} Q_j\right)^{0.3} \tag{48}$$

for outer ring. From this can calculate the basic reference rating life such that [21] p. 9

$$L_{10r} = \left[\left(\frac{Q_{ci}}{Q_{ei}}\right)^{-10/3} + \left(\frac{Q_{co}}{Q_{eo}}\right)^{-10/3}\right]^{-0.9} \tag{49}$$

where subscript 10 indicates the 90% reliability, like it does in the basic rating life calculation, and *r* refers to reference. Modified reference rating life for ball bearings is calculated in the same manner as the basic rating life, we only have to calculate the dynamic equivalent reference load such that [21] p. 9

$$P_{ref} = \frac{C}{L_{10r}^{1/3}} \tag{50}$$

and the modified refence rating life ball bearings such that

$$L_{nmr} = a_1 a_{ISO}\left(\frac{C}{P_{ref}}\right)^3 \tag{51}$$

Values for a_1 and a_{ISO} are calculated according to Chapter 3.1.2. Next, we go through calculations for roller bearings.

Now that the load distribution inside the bearing is known, we need to solve the pressure distributions for the roller-raceway contacts as it is required by ISO/TS 16281 to calculate reference rating lives for roller bearings. For this purpose, ISO/TS 16281 (technical specification) suggest using a method where the contact area is covered by a rectangular blanket, which is in turn divided into smaller rectangular elements. Pressure over the smaller elements is assumed to be even and the pressures for each element are then calculated such that [23] p. 53, 54

$$\left(\frac{1-\nu_1^2}{\pi E_1}-\frac{1-\nu_2^2}{\pi E_2}\right)\sum_{i=1}^{i=n_{elems}} f_{i,j}\sigma_i = \delta_j \tag{52}$$

On the left side of the summation the constant v is Poisson's coefficient and E is Young's modulus. Subscripts refer to bodies in contact. Inside the summation f is the influence of element i to element j, σ is the pressure over the element and δ is deformation over the element. Summation is over the number of elements in the blanket. This approach can be problematic as it requires extensive knowledge about the geometry of rolling elements and raceways, which is considered proprietary information by the bearing manufacturers, to be able to map deformations for the contacts.

However, information about roller and raceway profiles is more readily available and ISO/TS 16281 even provides reference geometries to substitute lacking knowledge [21] p. 12, 17, 18. This can be utilized when we use a lamina-based approach, where our roller is divided into slices called lamina. Using AST (alternative slicing technique) presented by Teutsch and Sauer, we only need to consider deformation at the centerline of contact, which can be modeled as interpenetration [24] p. 440.

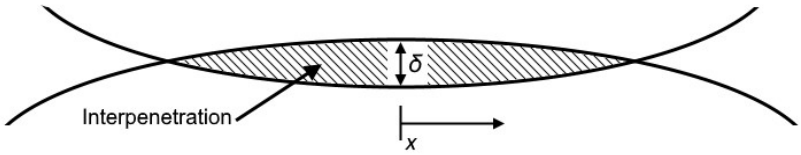

Figure 6. *Interpenetration of two bodies*

Interpenetration is determined by overlapping the contacting bodies by the amount of deformation calculated for that specific contact with Equation (34), such as in Figure 6. When profiles of the bodies are known, we can determine interpenetration in all points along x-axis. In bearings modeled with line contacts, the raceways were assumed to be unprofiled.

In roller bearings with point contacts, the contact deformation field was modeled as an ellipse [6] p. 108 with the height from Equation (34) and width 2a. Dimensionless half-length of the contact a^* was determined based on [6] p. 110 Table 6.1 from curvature difference F_ρ with linear interpolation for values in between those stated in the table. Actual major half-length of contact for steel bodies can be then calculated such that

$$a = 0.0236a^*\left(\frac{Q}{\sum\rho}\right)^{1/3} \tag{53}$$

Now that we can determine the deformations for each lamina, we need to calculate the influence coefficients. Lamina is term used discrete cylindrical slices of the roller used to analytically solve the rolling contact problem, somewhat similarly we would dissect a body to elements in tradition finite element analysis.

First, we need to determine constants c_i and c_o, for inner and outer ring contacts respectively, such that

$$c_i = 3.17\left(\frac{D_{pw}}{2}\right)^{1-m_{AST}}\left(\frac{1-\nu^2}{E}\right)^{m_{AST}} \tag{54}$$

$$c_o = 2.66\left(\frac{t}{1+\frac{D_{we}}{D_{pw}}}\right)^{1-m_{AST}}\left(\frac{1-\nu^2}{E}\right)^{m_{AST}} \tag{55}$$

where t is the combined thickness of outer raceway and housing. The width of a lamina is calculated such that

$$l_{ns} = \frac{L_{we}}{n_s} \tag{56}$$

where n_s is the number of equal width laminae the roller is divided to and m_{AST} is a specific exponent for inner and outer ring contacts. For inner ring contact m_{AST} = 0.92 and for outer ring contact

m_{AST} = 0.91. Now we can calculate elastic compliance *s* for inner ring and *s* for outer ring contact such that [24] p. 439

$$s = \frac{c^{1/m_{AST}}}{l_{ns}} \tag{57}$$

Influence *w* of lamina *j* to lamina *k* can be calculated such that [24] p. 440

$$\begin{aligned} w_{j,k} &= \left(\frac{1}{|x_j - x_k|}\right)^{1/m_{AST}}, j \neq k \\ w_{j,k} &= \left(\frac{4}{l_{ns}}\right)^{1/m_{AST}}, j = k \end{aligned} \tag{58}$$

where *x* is the coordinate of lamina center. For the solution, influence coefficient should be normalized with the average of all influence coefficients. Now we can solve the load for each lamina at inner and outer ring contacts such that [24] p. 439

$$s\frac{n_s^2}{\sum_{j,k} w_{j,k}} \sum_{k=1}^{n_s} w_{j,k} q_k = \delta_j^{1/m_{AST}}, j = 1 \dots n_s \tag{59}$$

where q_k is the load on lamina *k* and δ_j is deformation at lamina *j* [1]. Equation (59) should satisfy condition

$$Q_j = \sum_{k=1}^{n_s} q_k \tag{60}$$

where Q_j is the load on rolling element *j*. The linear equation system formed from Equation (59) can be then solved by computational means. Once we have solved to lamina loads on both contacts for all rollers, we can calculate the dynamic equivalent load on lamina such that

$$q_{kei} = \left(\frac{1}{Z}\sum_{j=1}^{Z} q_{j,k}^4\right)^{0.25}, k = 1 \dots n_s \tag{61}$$

for inner ring and

$$q_{keo} = \left(\frac{1}{Z}\sum_{j=1}^{Z} q_{j,k}^{4.5}\right)^{2/9}, k = 1 \dots n_s \tag{62}$$

for outer ring [21] p. 15. We also need to calculate the equivalent load for basic dynamic load rating in the same vein we did with the ball bearings such that [21] p. 13, 14

$$Q_c = \frac{1}{\lambda v}\frac{C}{b_2}\left\{1 + \left[b_3\left(\frac{1-\gamma}{1+\gamma}\right)^{143/108}\right]^{c_1}\right\}^{2/9} \tag{63}$$

Values for the coefficients in Equation (63) can be found from Table 7.

[1] In reference [24] Equation (18) the number of laminae is not squared, but the text references the influence coefficient being “normalized by the mean of all weighting functions”. For this reason the equation was modified to the form it is presented in this work.

Table 7. *Values for basic dynamic load rating equivalent load calculation for roller bearings*

		b_2	b_3	c_1	λv
Inner ring (Q_{ci})	rrb	$0.378Z\cos(\alpha)i^{7/9}$	1.038	9/2	0.83
	trb, $\alpha \neq 90°$	$Z\sin(\alpha)$	1	9/2	0.73
	trb, $\alpha = 90°$	Z	1	9/2	0.73
Outer ring (Q_{co})	rrb	$0.364Z\cos(\alpha)i^{7/9}$	1.038	-9/2	0.83
	trb, $\alpha \neq 90°$	$Z\sin(\alpha)$	1	-9/2	0.73
	trb, $\alpha = 90°$	Z	1	-9/2	0.73

Since the calculation for roller bearings is based on laminae, we need to calculate the basic dynamic load rating equivalent load for a lamina, instead of the whole roller, such that

$$q_{ci} = Q_{ci}\left(\frac{1}{n_s}\right)^{7/9} \tag{64}$$

for inner ring laminae and

$$q_{co} = Q_{co}\left(\frac{1}{n_s}\right)^{7/9} \tag{65}$$

for outer ring laminae. Now we can calculate the basic reference rating life such that [21] p. 16

$$L_{10r} = \left\{\sum_{k=1}^{n_s}\left[\left(\frac{q_{ci}}{q_{kei}}\right)^{-4.5} + \left(\frac{q_{co}}{q_{keo}}\right)^{-4.5}\right]\right\}^{-8/9} \tag{66}$$

Modified reference bearing life is calculated such that

$$L_{nmr} = a_1\left(\sum_{k=1}^{n_s}\left\{\left[a_{iso}\left(\frac{e_C C_u}{P_{ks}}\right)\right]^{-9/8}\left[\left(\frac{q_{ci}}{q_{kei}}\right)^{-4.5} + \left(\frac{q_{co}}{q_{keo}}\right)^{-4.5}\right]\right\}\right)^{-8/9} \tag{67}$$

Reliability factor is calculated as described in Chapter 3.1.2 as well as a_{ISO}, with the exception of dynamic equivalent load P_{ks}. Dynamic equivalent load for lamina k is calculated such that

$$P_{ks} = 0.323iZ\cos(\alpha)n_s\left\{\left[q_{kei}^{4.5} + \left(1.038\frac{q_{ci}}{q_{co}}\right)^{4.5} q_{keo}^{4.5}\right]\Big/\left[1 + \left(1.038\frac{q_{ci}}{q_{co}}\right)^{4.5}\right]\right\}^{2/9} \tag{68}$$

for radial roller bearings[2] and

$$P_{ks} = Z\sin(\alpha)n_s\left(\frac{q_{kei}^{4.5} + q_{keo}^{4.5}}{2}\right)^{2/9} \tag{69}$$

for thrust roller bearings [21] p. 16, 17.

3.1.4 Combined Fatigue Life

Methodologies for bearing fatigue life prediction assume constant operational and loading conditions for the bearing through its lifetime. In real world operations conditions for load, speed of revolution, lubrication, contamination etc. are changing constantly, so we must be able to combine the predictions for different conditions. For this we can utilize the Palmgren-Miner damage rule or Miner's damage rule such that [26] p. 160

[2] In reference [21] Equation (69) Z indicates the total number of rollers instead of number of rollers per row. If one tries to calculate equivalent load with the number rollers per row, in the experience of the author of this paper, the results are incorrect. In ISO/TS 16281 Z is used to mark both total number of roller and number of roller per row. For this reason the equation is modified in this work for more consistent notation.

$$\sum_{i=1}^{k} \frac{n_{ci}}{L_{ni}} = D \tag{70}$$

where the ratio of the number of cycles n_c and fatigue life L_n is summed over number of load cases k to calculate total amount of damage D. Then we can substitute damage D with ratio of sum of cycles to combined rating life and solve it for combined rating life such that [25] p. 12

$$L_{n,combined} = \frac{\sum_{i=1}^{k} n_{ci}}{\sum_{i=1}^{k} \frac{n_{ci}}{L_{ni}}} \tag{71}$$

This is the formulation most commonly found in bearing manufacturer catalogues.

3.2 Bearing Tool

The bearing fatigue tool procedure was separated into three sections: contact pressure calculations, load binning and fatigue damage calculation. The contact pressure calculation is only performed once for a specific bearing and loading bin configuration when the binning and fatigue damage calculation is performed each batch of loading data. In the case of ball bearings, pre-calculation of contact line pressures is not required as part of the ISO 16281 calculation scheme. This is not required for the basic bearing calculation scheme either, but the load binning is essentially identical for all bearing types and calculation schemes.

The pre-calculation of contact pressures includes calculating the load distribution for each roller Q_k and based on that the contact pressures for each roller laminae at inner and outer ring contacts $q_{j,k}$. Based on the contact pressures we can calculate the dynamic equivalent load for inner q_{kei} for inner ring and q_{keo} for outer ring using equations (61) and (62). And finally, basic dynamic load rating q_{ci} for inner ring and q_{co} for outer ring contact with equations (63) to (65). These four values are what are saved into a .csv -file, which is essentially a reduced order model (ROM). The primary function of this exercise is to save on calculation time, by performing the most time consuming part beforehand.

For us to be able to create the ROM, our load spectrum needs to be predetermined and static. This comes in from the load binning where we have chosen to divide the loading into hundred predetermined bins. The ROM generation process is described in Figure 7. The hundred bins are created such that we a have a range from zero to ten times nominal load and the hundred are evenly distributed along it. The goal is to create such a bin spectrum that our largest bin never gets any loading counted into it, since that last bin includes all loading that exceeded the limit all the way into infinity.

In the bearing tool, the counted loading is not based on cycles in the traditional sense, where a cycle consists of a changing load, but rather we count revolutions of the bearing and per static loading amount. This comes from definition of the standard where the loading is defined as a static load carried by the bearing. The amount of revolutions is determined from the time series signal based on the time delta between points, the speed of revolution, and the loading amount is the maximum of the two time series points in question. The amount of cycles is then summed into the appropriate bin.

After the bin counting, we can solve the accumulated damage value for each bin using our desired calculation method, appropriate for the bearing type. If we are using modified bearing life models, we also need to calculate life modification factor a_{ISO}. When modified bearing life models are used, lubricant viscosity and contamination are assumed to be constant through the whole batch of data. Associating each time sample with a matching viscosity/contamination value, would complicate the data structure considerably. Since the value for oil viscosity and contamination don't typically change very much during our relatively short batch times of 15 minutes, the gains from introducing this sort of fidelity to the bin counting was deemed unnecessary. The calculation procedure is described in Figure 8.

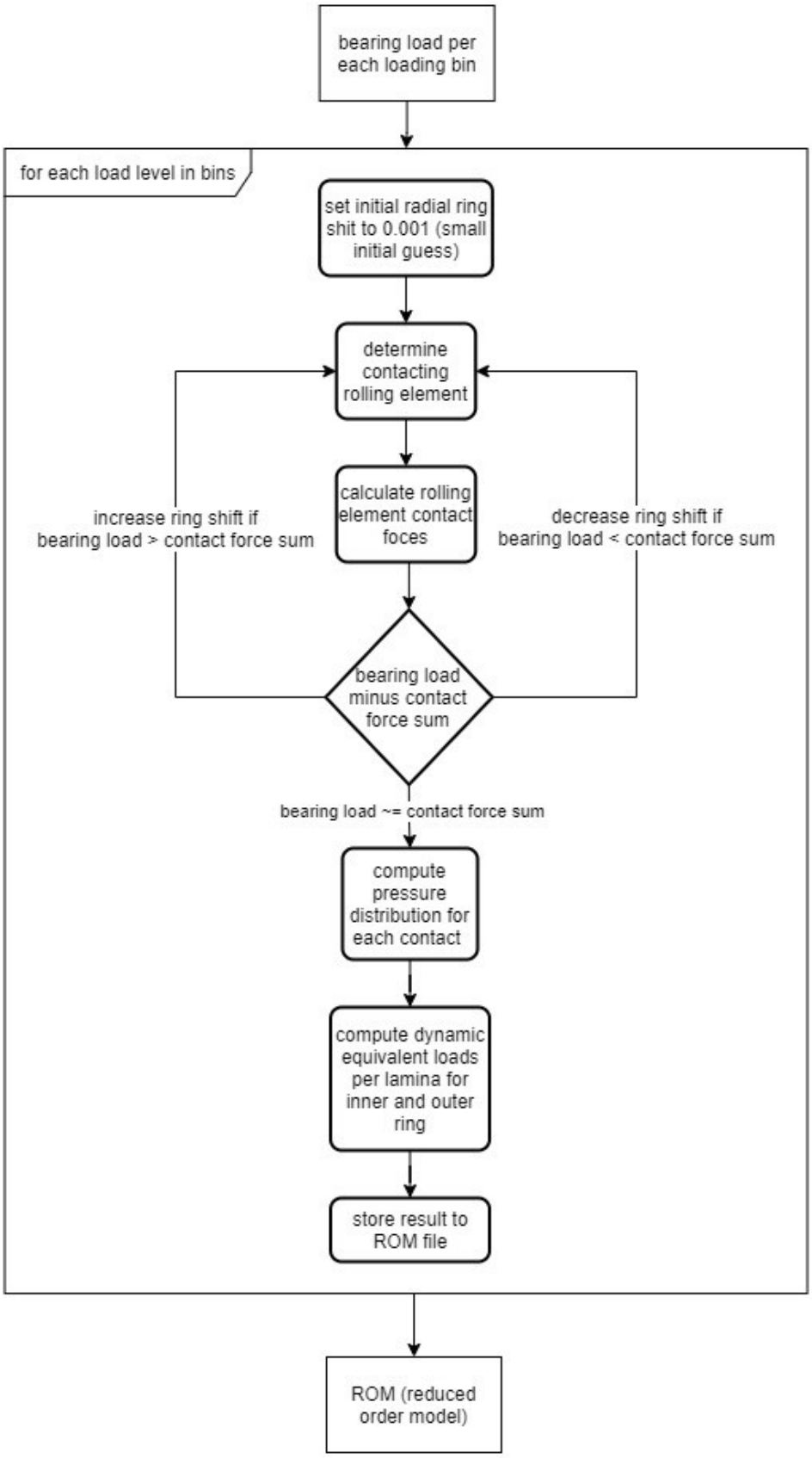

Figure 7. *ROM generation*

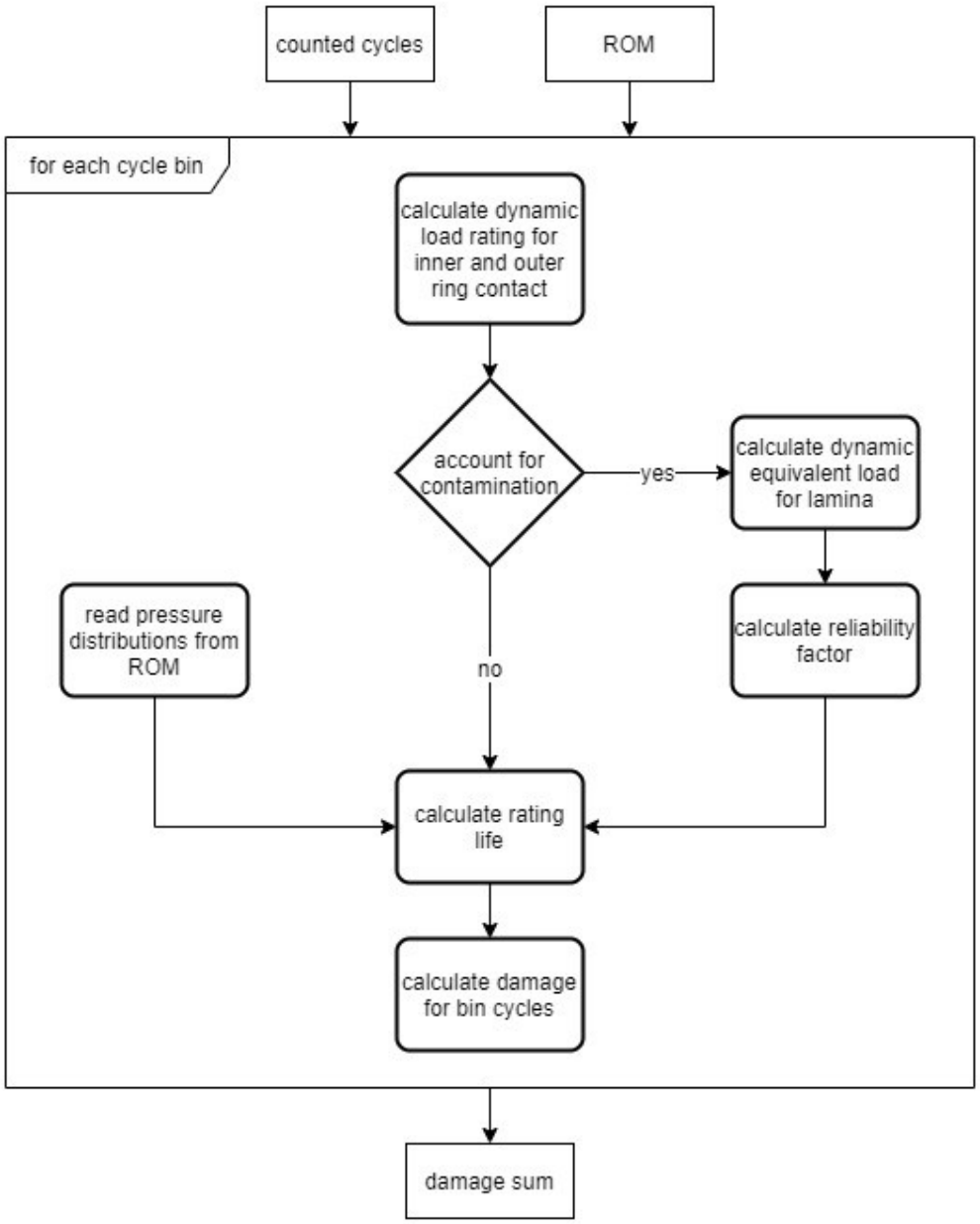

Figure 8. *Bearing fatigue calculation*

4. SHAFT MODEL

In this chapter we define the fatigue model for shafts based on the DIN 743 standard. Since DIN 743 is designed to calculate safety factors against different loading scenarios, a modification is made in an effort to produce damage values instead to better adapt it to the digital twin application. We also need to feed the model with means and amplitudes of the loading stress and for this a rainflow counting algorithm is used. In the end we also have a brief description of the fatigue damage counting program written in Python 3.

In the scope of this work, calculations are conducted according to DIN 743-1 load case 2 as it is described as the more general one. Load case 2 assumes relation of combined stress, tension compression and bending stress amplitude, and/or relation of combined stress shear component and torsion stress amplitude are constant regardless of load [27] p. 12, 13.

4.1 Theory

Fatigue life prediction for shaft according to DIN 743 is done by analyzing critical cross sections. A critical cross section can be defined anywhere on the shaft but typically they are located at notches, shoulders or other locations where there is a sudden change in the cross section of a shaft. Analysis can also be conducted on a smooth portion of a shaft, if needed. Loading for the shaft is considered in three directions: tension/compression, bending and torsion. To calculate the fatigue safety, we first need to determine three constants per loading direction for our shaft cross section, which are: fatigue limit, stress influence factor and yield point.

Fatigue limit for a shaft is determined as the maximum stress amplitude the material can endure under reversed stress condition without taking any damage.

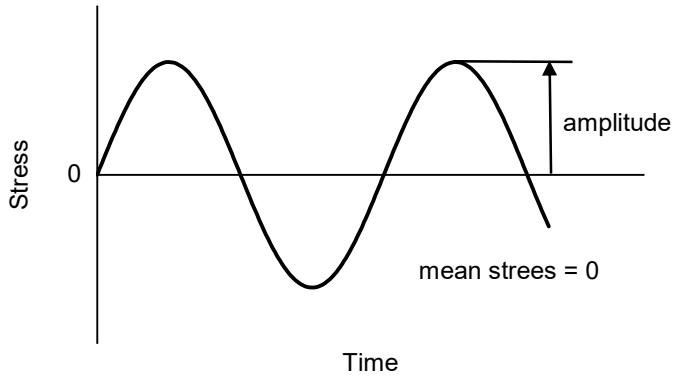

Figure 9. *Reversed stress loading*

A simple case of reversed stress loading can be represented with a sine wave shape and zero mean stress, such as it is depicted in Figure 9. Fatigue limit for a shaft point is calculated from a reference fatigue limit based on heat treatment, size of the component, geometry of the critical cross section (e. g. shoulder, notch, through hole), surface roughness, hardening and residual stresses for each loading direction such that [27] p. 10, 11

$$\sigma_{zdWK} = \frac{\sigma_{zdW}(d_B) \cdot K_1(d_{eff})}{K_\sigma} \tag{72}$$

$$\sigma_{bWK} = \frac{\sigma_{bW}(d_B) \cdot K_1(d_{eff})}{K_\sigma} \tag{73}$$

$$\tau_{tWK} = \frac{\tau_{tW}(d_B) \cdot K_1(d_{eff})}{K_\tau} \tag{74}$$

for tension/compression, bending and torsion, respectively. In the aforementioned equations, and in other notation regarding shafts, subscript *zd* refers to tension/compression, *b* to bending and *t* to torsion. Fatigue limits σ_{zdW}, σ_{bW} and τ_{tW} are fatigue limits for test bar of diameter d_b. These fatigue limits can be determined via testing or one can use values provided in [29]. Factor K_1 is the technological influence factor for effective cross section diameter for heat treatment d_{eff} determined based on [28] Chapter 6.2. Combined influence factors K_σ for compression/tension and bending, and K_τ torsion combines the effects of notch geometry and surface quality such that

$$K_\sigma = \left(\frac{\beta_\sigma}{K_2(d)} + \frac{1}{K_{F\sigma}} - 1\right)\frac{1}{K_V} \tag{75}$$

$$K_\tau = \left(\frac{\beta_\tau}{K_2(d)} + \frac{1}{K_{F\tau}} - 1\right)\frac{1}{K_V} \tag{76}$$

Geometrical influence factor K_2 for notch diameter d can be determined based on [28] p. 26. This takes into consideration the fact that bending and torsion fatigue limits move closer to the tension/compression limit as the size increases. Influence factor for surface roughness $K_{F\sigma}$, $K_{F\tau}$ takes into considerations the effects of surface roughness and it can be determined based on [28] Chapter 7. Lastly, influence factor for surface conditioning K_V takes into account the effects of surface treatments such as heat treatments and mechanical surface hardening like shot peening. This factor can be determined based on [28] Chapter 8.

Fatigue notch factor β_σ, β_τ is determined as a stress ration between a notched and unnotched bar such that [28] p. 6

$$\beta_\sigma = \frac{\sigma_{zdW}(d)}{\sigma_{zdWK}} \tag{77}$$

$$\beta_\sigma = \frac{\sigma_{bW}(d)}{\sigma_{bWK}} \tag{78}$$

$$\beta_\tau = \frac{\tau_{tW}(d)}{\tau_{tWK}} \tag{79}$$

Since determining the fatigue limit for specific notches to utilize Equation (77) is not practical due to the need of time consuming fatigue testing, fatigue notch factor is generally calculated from reference notch geometries or from stress concentration factors. Stress concentration factor is the relative increase in stress at the notch such that [33] p. 1

$$\alpha_\sigma = \frac{\sigma_{max}}{\sigma_{nom}} \tag{80}$$

$$\alpha_\tau = \frac{\tau_{max}}{t_{nom}} \tag{81}$$

where σ_{max} and τ_{max} are the maximum principal stress and maximum shear stress at the notch. Denominators σ_{nom} and τ_{nom} are nominal stresses on the shaft. Stress concentration factors can using Equation (80) along with FEM (Finite Element Method) to calculate the maximum principal stress of an arbitrary notch or from mathematical models defined for different geometries found from literature, such as those from references [28] Chapter 5 or [33]. Once the stress concentration factor is determined, fatigue notch factor can be calculated such that

$$\beta_\sigma = \frac{\alpha_\sigma}{s_n} \tag{82}$$

$$\beta_\tau = \frac{\alpha_\tau}{s_n} \tag{83}$$

where sensitivity factor s_n is calculated such that

$$s_n = 1 + \sqrt{G'} \cdot 10^{-\left(0.33\frac{\sigma_S(d)}{712}\right)} \tag{84}$$

for heat treated, normalized or non-carbonized case-hardened shaft and

$$s_n = 1 + \sqrt{G'} \cdot 10^{-0.7} \tag{85}$$

for shafts with hardened surfaces [28] p. 12, where $\sigma_{S(d)}$ is yield strength of diameter d bar and G' is the relative stress gradient. Formulation for relative stress gradient depends on the notch geometry and it can be calculated using [28] Section 4.3. Fatigue notch factor can be alternatively solved from reference diameter d_{BK} fatigue notch factors $\beta_\sigma(d_{BK})$, $\beta_\tau(d_{BK})$ such that [28] p. 6

$$\beta_\sigma = \beta_\sigma(d_{BK}) \frac{K_3(d_{BK})}{K_3(d)} \tag{86}$$

$$\beta_\tau = \beta_\tau(d_{BK}) \frac{K_3(d_{BK})}{K_3(d)} \tag{87}$$

where K_3 is a geometrical influence factor that takes into consideration the changes in notch fatigue factor with the changes in shaft size. Influence factor K_3 can be determined according to [28] Chapter 6.4. Reference fatigue notch factors for different notch and shoulder geometries can be calculated according to [28] Chapter 4.2.

Yield points tension/compression and bending can be calculated such that [27] p. 16

$$\sigma_{zdFK} = K_1(d_{eff}) K_{2F} \gamma_F \sigma_S(d_B) \tag{88}$$

$$\sigma_{bFK} = K_1(d_{eff}) K_{2F} \gamma_F \sigma_S(d_B) \tag{89}$$

where K_{2F} is the static support factor according to [27] p. 17 Table 3, γ_F is the increase factor according to [27] p. 17 Table 2 and σ_S is the yield strength value for a bar with reference diameter d_B, which can be determined experimentally or from [29]. Fatigue strength for torsion is then determined from the Equation (88) such that [27] p. 16

$$\tau_{tFK} = \frac{\sigma_{zdFK}}{\sqrt{3}} \tag{90}$$

which is according to the von Mises yield criterion that states fatigue strength for principal stress is √3 times that of the shear [32] see [31].
Lastly, we need to calculate influence factors for mean stress sensitivity such that [27] p. 14

$$\psi_{zd\sigma K} = \frac{\sigma_{zdWK}}{2K_1(d_{eff}) \cdot \sigma_B(d_B) - \sigma_{zdWK}} \tag{91}$$

$$\psi_{b\sigma K} = \frac{\sigma_{bWK}}{2K_1(d_{eff}) \cdot \sigma_B(d_B) - \sigma_{bWK}} \tag{92}$$

$$\psi_{\tau K} = \frac{\tau_{tWK}}{2K_1(d_{eff}) \cdot \sigma_B(d_B) - \tau_{tWK}} \tag{93}$$

Now that the constants for the notch are calculated, we need to need to determine the combined mean stress for our loading cycles [27] p. 14. Combined mean stress is calculated according to von Mises stress [27] p. 14 [31] see [32]

$$\sigma_{mv} = \sqrt{0.5[(\sigma_{11} - \sigma_{22})^2 + (\sigma_{22} - \sigma_{33})^2 + (\sigma_{33} - \sigma_{11})^2 + 6(\sigma_{12}^2 + \sigma_{23}^2 + \sigma_{31}^2)]} \tag{94}$$

Since in we only have stresses in the axial directions and torsional stress, we can write Equation (94) such that

$$\sigma_{mv} = \sqrt{\sigma_{11}^2 + 3\sigma_{23}^2} \tag{95}$$

Tension/compression and bending contribute stress in the same direction so we can write Equation (95) such that

$$\sigma_{mv} = \sqrt{(\sigma_{zdm} + \sigma_{bm})^2 + 3\tau_{tm}^2} \tag{96}$$

where σ_{zdm} is the mean tension/compression stress, σ_{bm} is the mean bending stress and τ_{tm} is the mean torsion stress. Shear component of the mean stress can be then calculated

$$\tau_{mv} = \frac{\sigma_{mv}}{\sqrt{3}} \tag{97}$$

from the von Mises stress [27] p.14.
However, in the case $\sigma_{zdm} + \sigma_{bm} < 0$, combined mean stress is calculated such that [27] p. 13

$$\sigma_{mv} = \frac{H}{|H|}\sqrt{|H|}, \tag{98}$$

where parameter *H* is substituted with

$$H = \frac{(\sigma_{zdm} + \sigma_{bm})^3}{|\sigma_{zdm} + \sigma_{bm}|} + 3\tau_{tm}^2. \tag{99}$$

Since our fatigue limit is calculated for a reversed stress loading, we need to calculate the actual damaging amplitude based on the mean combined stress. Method of calculation per loading direction depends on a specific condition per direction such that

$$\frac{\sigma_{mv}}{\sigma_{zda}} \leq \frac{\sigma_{zdFK} - \sigma_{zdWK}}{\sigma_{zdWK} - \sigma_{zdFK}\psi_{zd\sigma K}} \tag{100}$$

for tension/compression,

$$\frac{\sigma_{mv}}{\sigma_{ba}} \leq \frac{\sigma_{bFK} - \sigma_{bWK}}{\sigma_{bWK} - \sigma_{bFK}\psi_{b\sigma K}} \tag{101}$$

for bending and

$$\frac{\tau_{mv}}{\tau_{ta}} \leq \frac{\tau_{tFK} - \tau_{tWK}}{\tau_{tWK} - \tau_{tFK}\psi_{tK}} \tag{102}$$

for torsion. In the aforementioned inequalities σ_{zda}, σ_{ba} and τ_{ta} are stress amplitudes. If a condition in Inequalities (100) to (102) is fulfilled for a particular load direction, damaging amplitude for that particular direction can be calculated such that

$$\sigma_{zdADK} = \frac{\sigma_{zdWK}}{1 + \psi_{zd\sigma K}\frac{\sigma_{mv}}{\sigma_{zda}}} \tag{103}$$

$$\sigma_{bADK} = \frac{\sigma_{bWK}}{1 + \psi_{b\sigma K}\frac{\sigma_{mv}}{\sigma_{ba}}} \tag{104}$$

$$\tau_{tADK} = \frac{\tau_{tWK}}{1 + \psi_{tK}\frac{\tau_{mv}}{\tau_{ta}}} \tag{105}$$

When a condition in Inequalities (100) to (102) is not satisfied, damaging amplitude is calculated such that [27] p. 13

$$\sigma_{zdADK} = \frac{\sigma_{zdWK}}{1 + \frac{\sigma_{mv}}{\sigma_{zda}}} \tag{106}$$

$$\sigma_{bADK} = \frac{\sigma_{bWK}}{1 + \frac{\sigma_{mv}}{\sigma_{ba}}} \tag{107}$$

$$\tau_{tADK} = \frac{\tau_{tWK}}{1 + \frac{\tau_{mv}}{\tau_{ta}}} \tag{108}$$

Fatigue safety against loading can be then calculated such that [27]

$$S_C = \frac{1}{\sqrt{\left(\frac{\sigma_{zda}}{\sigma_{zdADK}} + \frac{\sigma_{ba}}{\sigma_{bADK}}\right)^2 + \left(\frac{\tau_{ta}}{\tau_{tADK}}\right)^2}} \tag{109}$$

Fatigue safety factor describes the margin of loading we have against the load limit at the required number of fatigue cycles. DIN 743-1 suggests a factor of safety of 1.2, but in the scope of this

work, fatigue damage starts to accumulate when safety factor reaches 1. Safety factor limit of one was chosen for this thesis based on past experiences at Kongberg, but it can be almost arbitrarily set to any value depending on how sensitive we want the damage accumulation to be.

Since DIN 743 for multidirection load cases only calculates the safety against fatigue, we need to formulate a scheme, that calculates the accumulated fatigue damage in cases our loading amplitude exceeds that of the damaging amplitude. This can be achieved with a use of a Wöhler or S-N curve. In the scope of this thesis, load cases being multi directional means the combined stress calculated from three different loading directions as described in the start of this section. The multiple directions of the load case cause most issues in the cycle counting part where it is difficult to retain synchronicity between different sections. This is further discussed in Sections 4.2 and 4.3.

DIN 743-4 determines the Wöhler curve such that low cycle limit N_S is 10^3 cycles and high cycle limit N_D is 10^6 cycles [30] p. 6. platous at the beginning and the end of the curve are horizontal. Since we are dealing with a multidirectional loading case, we need to determine our Wöhler curve in terms of number of cycles and safety factor, instead of the more commonly used stress. To fully define our Wöhler curve we need to calculate the damaging amplitudes for N_S cycles for tension/compression, bending and torsion such that

$$\sigma_{zdASK} = \sqrt[b_w]{\frac{N_D}{N_S}}\sigma_{zdADK} \tag{110}$$

$$\sigma_{bASK} = \sqrt[b_w]{\frac{N_D}{N_S}}\sigma_{bADK} \tag{111}$$

$$\tau_{tASK} = \sqrt[b_w]{\frac{N_D}{N_S}}\tau_{tADK} \tag{112}$$

where b_w is the Wöhler curve exponent. Wöhler curve exponent for tension/compression and bending is 5 and 8 for torsion [30] p. 6. Now we can calculate the safety factor for a loading that would result in a safety factor of one using Equation (109) against the amplitudes determined using Equations (110) to (112) such that

$$S_S = \frac{1}{\sqrt{\left(\frac{S_C\sigma_{zda}}{\sigma_{zdASK}} + \frac{S_C\sigma_{ba}}{\sigma_{bASK}}\right)^2 + \left(\frac{S_C\tau_{ta}}{\tau_{tASK}}\right)}} \tag{113}$$

Safety factor limit of one was chosen for this thesis, but it can be almost arbitrarily set to any value depending on how sensitive we want the damage accumulation to be. With this we can finally determine the function for the sloped portion of the Wöhler curve, which has the general form

$$y = c_w x^{1/b_w} \tag{114}$$

This is sometimes called a power function. Based on our two known points (N_S, S_S) and $(N_D, 1)$, we can solve constant c_w and exponent $1/b_w$ such that

$$c_w = S_S N_S^{\left(-\log \frac{1}{S_S}\right)^{\frac{1}{\log \frac{N_D}{N_S}}}} \tag{115}$$

$$\frac{1}{b_w} = \log\left[\left(\frac{1}{N_S}\right)^{\frac{1}{\log \frac{N_D}{N_S}}}\right] \tag{116}$$

Wöhler curve is fully defined and it can be plotted such as in Figure 10. It is assumed that, if the loading experienced by the shaft is over the fatigue limit, it is on the sloped part of the Wöhler curve and strength against yielding is checked separately. It should also be noted that in Figure 10 the inverse of the safety factor is used so that the origin for y-axis starts from zero for better readability.

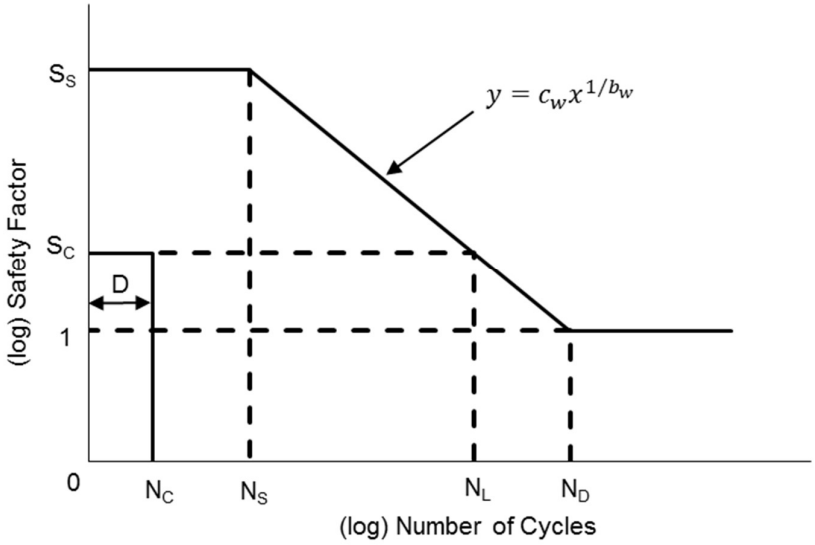

Figure 10.*Wöhler curve projected based on calculated knee points*

Thus we can calculate the maximum endurable cycles for loading from Equation (114) such that

$$N_L = \left(\frac{S_C^{-1}}{c_w}\right)^{1/b_w} \tag{117}$$

and then the inflicted damage according to the Miner's damage rule such that [26] p.

$$D = \frac{N_C}{N_L} \tag{118}$$

where N_C is the amount cycles for the particular loading. End of the fatigue life is reached when sum of damage for all cycles reaches 1. Safety against yielding can be calculated such that [27] p. 15

$$S_y = \frac{1}{\sqrt{\left(\frac{\sigma_{zdmax}}{\sigma_{zdFK}} + \frac{\sigma_{bmax}}{\sigma_{bFK}}\right)^2 + \left(\frac{\tau_{tmax}}{\tau_{tFK}}\right)}} \tag{119}$$

where σ_{zdmax}, σ_{bmax} and τ_{tmax} are maximum stresses for each direction. DIN 743-1 suggests a minimum safety factor of 1.2 [27] p. 14.

4.2 Rainflow Cycle Counting

To be able to utilize DIN 743 fatigue analysis, we need to extract stress ranges and means from loading cycles. From the stress-strain diagram in Figure 11, which is plotted according to [34] p. 91, cycles can be easily extracted such as they are in Table 9 since each cycle is clearly distinguishable by eye.

Table 8. *Stress-strain points*

	Time	Stress	Strain
A	1	4.00	0.043
B	2	-2.00	0.007
C	3	2.70	0.031
D	4	-4.00	-0.043
E	5	3.20	0.015
F	6	-2.00	-0.012
G	7	1.00	0.002
H	8	-3.00	-0.023
A	9	4.000	0.043

Table 9. *Cycles with stress and strain ranges from Figure 11*

	Cycle	A-B-A	B-C-B	E-H-E	F-G-F
Stress	Mean	0.00	0.35	0.10	-0.50
	Amplitude	8.00	4.70	6.20	3.00
Strain	Mean	0.000	0.012	0.004	-0.005
	Amplitude	0.086	0.024	0.038	0.014

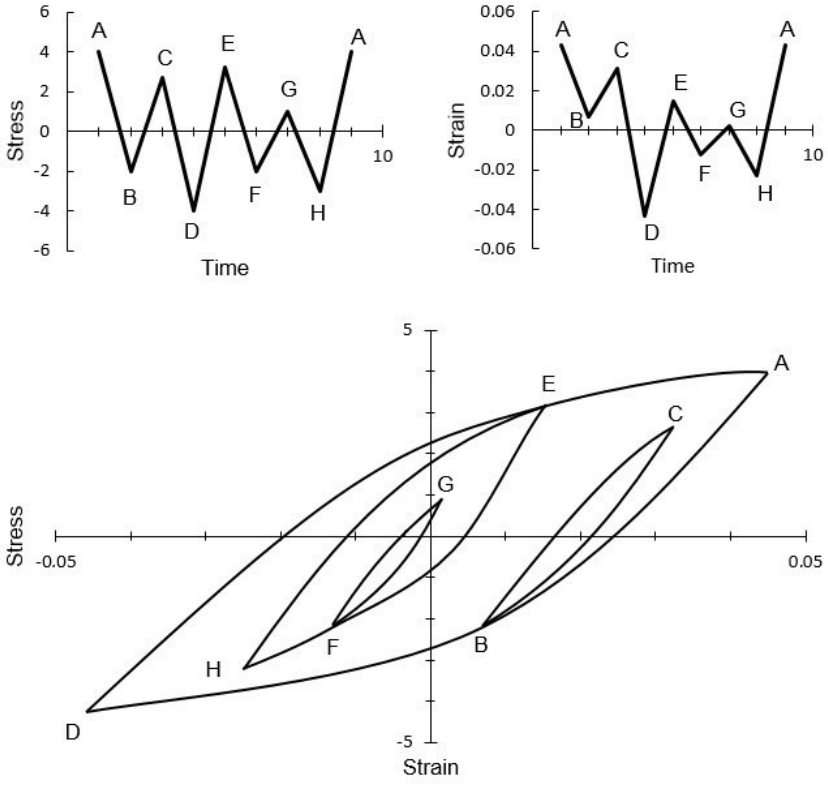

Figure 11. *Stress and strain histories with the stress-strain hysteresis loops plotted from Table 8*

The method for identifying and counting these stress or strain cycles was introduced by Matsuishi and Endo called the rainflow counting method [35]. The name comes from the analogy that

the history diagram is rotated 90° and then the water flows down from the reversal points to identify the cycles [34] p. 91. Figure 13, where stress diagram from Figure 11 is rotated, demonstrates this method. It should also be noted that in the case the loading history is continuous, reversal points should first be identified from the time series data. Reversal happened when the derivatives of point before and after it have a different sign, such as in Figure 12. It is also up to the discretion of the operator, whether or not the first and/or last point of the data is considered a reversal.

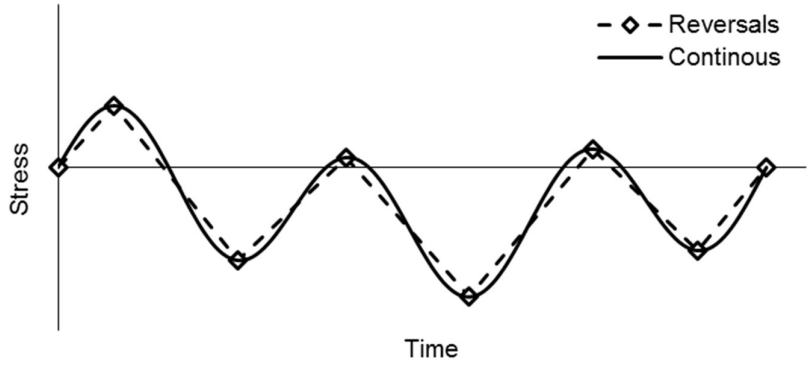

Figure 12.*Reversals from smooth data*

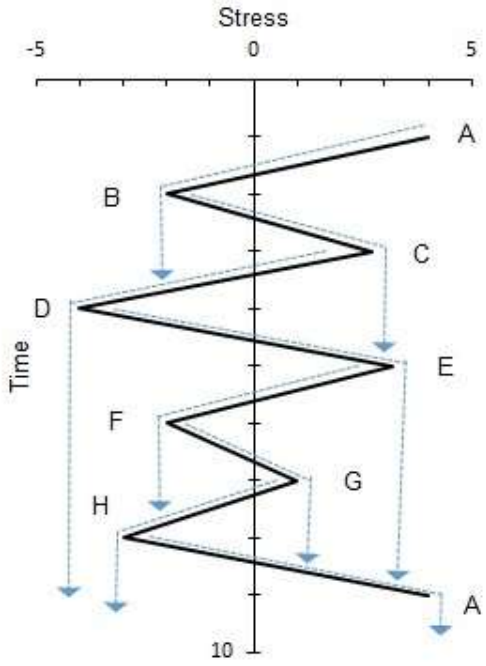

Figure 13. *Rotated stress diagram*

Cycles are then counted in accordance with the following scheme [34] p. 91, 92 see [35], with examples from Figure 13:

1. rainflow starts from top most reversal point
2. count a half-cycle when one of the following conditions
    a. flow falls to a section with a high absolute point (flow from B-C falls to flow from D-E)
    b. flow meets a flow falling from above (flow C-D meets the flow from A-B)
    c. flow falls completely off (flow A-D drops off at D)
3. go back to step 1 starting from the next reversal point unless all reversal points are handled
4. combine half-cycles with the same mean and amplitude

There are multiple different rainflow counting schemes developed for both uniaxial and multi-directional loading. For this work, the method described in ASMT International standard ASTM E 1049-85 [37] p. 3, 4 is used, which was in turn executed on each of the three loading directions [35] p. 113. This three-point counting technique was originally developed by Downing and Socie [36]. A multidirectional rainflow counting scheme called modified Wang-Brown method [38] [39] was also considered, but it wasn't clear without extensive research whether or not it would be applicable for DIN 743. Thus the Downing and Socie method was chosen due to time constrictions.

As its name might suggest, Downing and Socie method counts cycles by comparing three ranges of three reversal points to each other. These points are stored in stack-type data structure, such as the one in Figure 14.

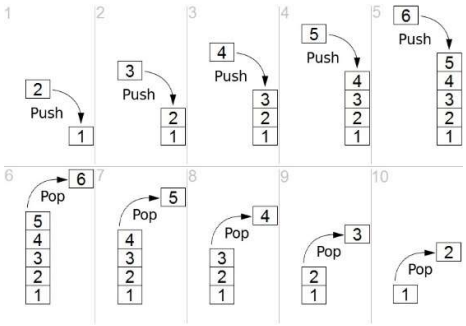

Figure 14. *Stack data structure*[3]

The three most recent points in order are then called *P1*, *P2* and *P3*, *P3* being the most recent one. These points are read from the beginning of the data and two ranges calculated such that [36] p. 32

$$RX = |P3 - P2| \tag{120}$$

$$RY = |P2 - P1| \tag{121}$$

If range *RX* ≥ *RY*, that range is counted as a half-cycle and the two most recent points are popped from the stack and two new points are from the loading diagram. In case the condition is not met, one new point is read from diagram to the stack and the loop repeats. This is repeated until all points are handled.

4.3 Shaft Tool

Damage calculation procedure for a particular shaft cross section is separated in two different parts: pre-damage calculation and damage calculation. In the pre-damage calculation step where we determine bending fatigue limits with equations (72) to (74), mean stress influence factor with equations (91) to (93) and material yield points with equations (88) to (90), for tension/compression, bending and torsion respectively. Since these values are only dependent on geometry and construction, we save these values into a .csv -file (Comma Separated Values) so we don't need calculate them over and over again when we do the damage calculation for separate time series data sets.

In the damage calculation phase we first need to determine stress amplitudes for the signed von Mises stress used using the rainflow cycle counting method described in section 4.2. Since our rainflow counting algorithm is only capable doing the calculation in a single direction at a time, we need to add time dependency for the three different signal some other way. We implement the time dependency by splitting the signal into ten second blocks and then cycle count the different signal within those blocks and assume them to be adequately correlated.

Since we can't be sure that all signal are in the same phase, the different signal can experience different amount of cycles and half cycles, we need to ensure that every subsection of the ten

[3] https://commons.wikimedia.org/wiki/File:Lifo_stack.png, retrieved 8.8.2019 under Creative Commons 1.0 Universal

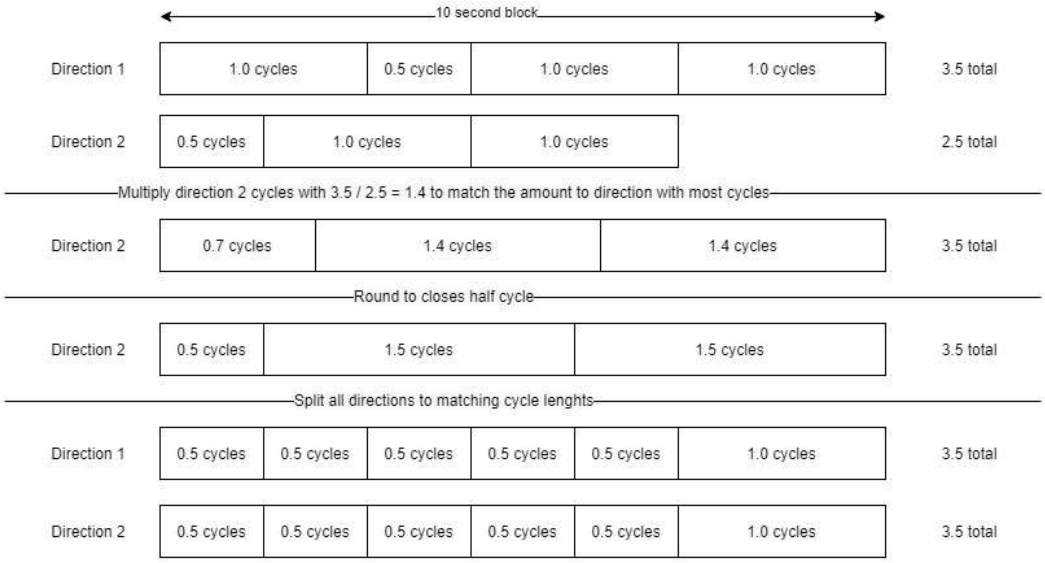

Figure 15.*Rainflow cycle matching*

second block has a stress range associated for each of the signals. To ensure this we scale all signal so that they have the same amount of total cycles as the one with most cycles for the current block. After scaling the amount of cycles is typically not a half or a full cycle but some other floating-point number. So that we once more have all cycle counts as half or full cycles we increase or decrease the count so that it matches the half/full cycle scheme. You can see process in Figure 15 for two direction, but additional directions can be added and matched similarly to direction 2.

Another feature of splitting the data into ten second blocks is that we usually don't do the split at a reversion point. To avoid missing cycles this way or counting the last point of the block as a reverse point, this last tail of the data is passed to the next ten second block and incorporated into it to avoid counting incorrect cycles or missing cycles. Even if we do pass the tail of the data this way, some cycles with long wave length might be missed, but those are assumed not to introduce unacceptable errors.

Based on the reversal points we get from the rainflow counting we calculate stress means and amplitudes and from those extract damaging amplitudes with equations (103) to (108) to calculate safety against high cycles fatigue with equation (109). If the loading condition is determined to be damaging, the accumulated damage is then calculated based on the number of cycles counted and the number of allowable cycle for the loading condition. Shaft calculation procedure with rainflow counting is described in Figure 16. All loading blocks are also checked against the yielding condition since if any there is any yielding in the shaft, the damage calculation is no longer necessary since we know that the shaft has already yielded.

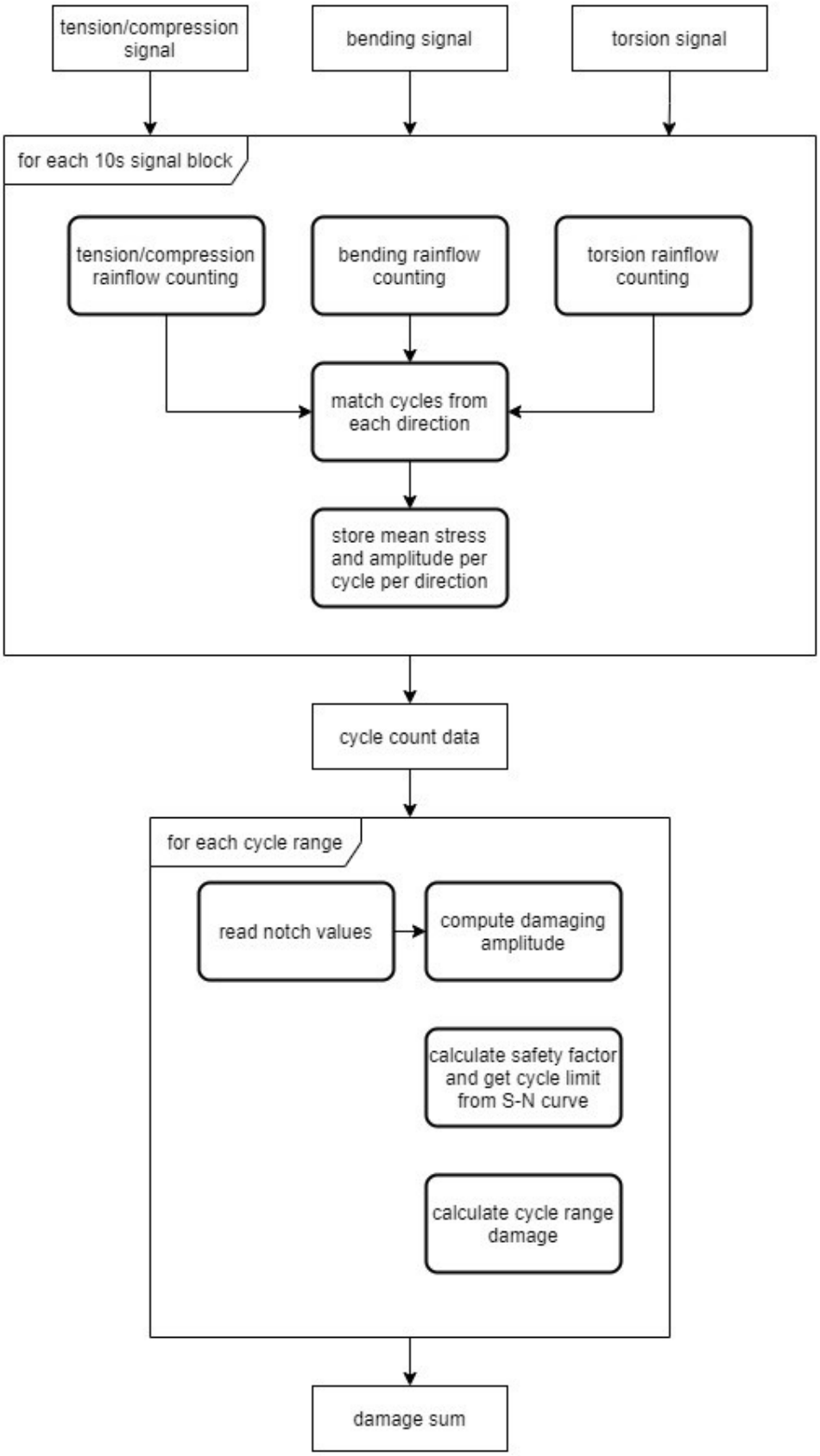

Figure 16.*Rainflow and shaft calculation procedure*

5. VERIFICATION

5.1 Bearing Tool Verification

The verification of the ISO 16281 Python module was done against Schaeffler BearinX. For radial bearings (RBBs and RRBs), load was applied only in the radial direction and for thrust bearings (TRBs), load was only applied in the axial direction respectively. For each bearing type, results for two different bearing types with ten different load levels were calculated.

Gathering input values for calculation is not as straight forward as one would like, since bearing manufacturers consider most of the values to be confidential. Values for basic calculations such as load ratings and external dimensions are readily available [40], but everything from number of rolling elements to contact geometries must be estimated. In BearinX, input values are read from a database, which is not visible to the user. Input values for the Python program are listed below in Table 10, Table 11 and Table 12.

Table 10. *Radial ball bearing inputs*

Bearing ID	6016	16028
Type	RBB	RBB
C (N)	51000	86000
C_U (N)	2410	3850
D_{pw} (mm)	102.500	175.431
α (°)	0	0
i	1	1
Z	14	19
r_b (mm)	6.75	8.34
$r_{i,1}$ (mm)	-7.02	-8.67
$r_{i,2}$ (mm)	44.50	79.17
$r_{o,1}$ (mm)	-7.15	8.84
$r_{o,2}$ (mm)	-58.00	-95.84
P_d (mm)	0.0056	0.0083

Table 11. *Radial roller bearing inputs*

Bearing ID	23056-BE-XL	NJ2220-BE-XL-TVP2
Type	RRB	RRB
C (N)	1780000	395000
C_U (N)	260000	77000
α (°)	8.5	0
α_i (°)	-	-
α_o (°)	-	-
i	2	1
Z	27	17
D_{pw} (mm)	353.400	141.000
D_{we} (mm)	35.000	22.000
L_{we} (mm)	35.230	60.100
r_r (mm)	192.300	-
r_i (mm)	198.510	-
r_o (mm)	196.300	-
t (mm)	16.0	9.0
P_d (mm)	0.0925	0.0368

Table 12. *Thrust roller bearing inputs*

Bearing ID	32228-XL	29436-E1-XL
Type	TRB	TRB
C (N)	760000	2850000
C_U (N)	140000	770000
α (°)	18.2	52
α_i (°)	16.2	-
α_o (°)	20.0	-
i	1	1
Z	20	16
D_{pw} (mm)	195.000	269.900
D_{we} (mm)	49.800	42.100
L_{we} (mm)	49.800	62.900
r_r (mm)	-	236.100
r_i (mm)	-	243.400
r_o (mm)	-	243.400
t (mm)	14.00	42.00
P_d (mm)	0	0

Fatigue life was then calculated at ten load points with the load increased linearly. For RBB the loading was placed around the fatigue load limit C_U of the bearing and around the half of the

fatigue load limit for TRB and RRB. The load points and comparative results can be found in Table 13, Table 14 and Table 15.

Table 13. *Radial ball bearing results*

			Reference Rating Life L10r (10^6)			Modified Reference Rating Life L10rm (10^6)		
Bearing ID	Type	Load (N)	BearinX	Python	Diff. (%)	BearinX	Python	Diff. (%)
6016	RBB	2100	13070	13092	0.168 %	653600	654603	0.153 %
		2400	8825	8834	0.102 %	441300	441720	0.095 %
		2700	6238	6241	0.048 %	311900	312071	0.055 %
		3000	4571	4572	0.022 %	228600	228631	0.014 %
		3300	3450	3450	0.000 %	146500	159482	8.861 %
		3600	2667	2667	0.000 %	89360	96804	8.330 %
		3900	2105	2104	-0.048 %	57310	61827	7.882 %
		4200	1690	1689	-0.059 %	38310	41178	7.486 %
		4500	1378	1377	-0.073 %	26510	28405	7.148 %
		4800	1138	1137	-0.088 %	18890	20187	6.866 %
16028	RBB	4200	7665	7984	4.162 %	383200	399217	4.180 %
		4600	5873	6103	3.916 %	293600	305180	3.944 %
		5000	4599	4770	3.718 %	230000	238528	3.708 %
		5400	3670	3799	3.515 %	183500	189972	3.527 %
		5800	2975	3075	3.361 %	136800	153762	12.399 %
		6200	2445	2524	3.231 %	93460	111412	19.208 %
		6600	2034	2097	3.097 %	65800	77821	18.269 %
		7000	1711	1761	2.922 %	47550	55846	17.447 %
		7400	1452	1493	2.824 %	35150	41026	16.717 %
		7800	1243	1277	2.735 %	26500	30763	16.087 %

Table 14. *Radial roller bearing results*

			Reference Rating Life L10r (10^6)			Modified Reference Rating Life L10rm (10^6)		
Bearing ID	Type	Load (N)	BearinX	Python	Diff. (%)	BearinX	Python	Diff. (%)
23056-BE-XL	RRB	100000	13040	17919	37.416 %	73740	108108	46.607 %
		110000	10040	13871	38.157 %	50500	74453	47.432 %
		120000	7900	10982	39.013 %	35840	53174	48.365 %
		130000	6337	8853	39.703 %	26210	39094	49.157 %
		140000	5171	7249	40.186 %	19690	29456	49.599 %
		150000	4275	6015	40.702 %	15100	22661	50.073 %
		160000	3575	5048	41.203 %	11790	17743	50.492 %
		170000	3012	4277	41.999 %	9307	14102	51.520 %
		180000	2568	3655	42.329 %	7480	11356	51.818 %
		190000	2204	3148	42.831 %	6072	9251	52.355 %
NJ2220-E-XL-TVP2	RRB	40000	7896	7642	-3.217 %	61000	52655	-13.680 %
		42000	6690	6574	-1.734 %	47310	42124	-10.962 %
		44000	5709	5682	-0.473 %	37170	33974	-8.598 %
		46000	4902	4937	0.714 %	29530	27651	-6.363 %
		48000	4235	4316	1.913 %	23720	22732	-4.165 %
		50000	3681	3790	2.961 %	19260	18825	-2.259 %
		52000	3218	3339	3.760 %	15790	15683	-0.678 %
		54000	2830	2959	4.558 %	13070	13189	0.910 %
		56000	2492	2632	5.618 %	10860	11156	2.726 %
		58000	2205	2351	6.621 %	9090	9495	4.455 %

Table 15. *Thrust roller bearing results*

			Reference Rating Life L10r (10^6)			Modified Reference Rating Life L10rm (10^6)		
Bearing ID	Type	Load (N)	BearinX	Python	Diff. (%)	BearinX	Python	Diff. (%)
32228-XL	TRB	40000	24730	21041	-14.917 %	301700	224586	-25.560 %
		44000	18210	15908	-12.641 %	187300	146834	-21.605 %
		48000	13710	12302	-10.270 %	121100	99795	-17.593 %
		52000	10560	9688	-8.258 %	81510	69961	-14.169 %
		56000	8277	7751	-6.355 %	56560	50377	-10.932 %
		60000	6584	6289	-4.481 %	40270	37126	-7.807 %
		64000	5317	5165	-2.859 %	29430	27916	-5.144 %
		68000	4346	4288	-1.335 %	21940	21361	-2.639 %
		72000	3595	3593	-0.056 %	16690	16596	-0.563 %
		76000	2998	3036	1.268 %	12860	13065	1.594 %
29436-E1-XL	TRB	200000	14240	11737	-17.577 %	26210	22485	-14.212 %
		220000	10700	8859	-17.206 %	18060	15567	-13.804 %
		240000	8235	6849	-16.831 %	12880	11151	-13.424 %
		260000	6478	5404	-16.579 %	9467	8218	-13.193 %
		280000	5182	4341	-16.229 %	7121	6209	-12.807 %
		300000	4223	3540	-16.173 %	5495	4788	-12.866 %
		320000	3476	2923	-15.909 %	4298	3757	-12.587 %
		340000	2894	2444	-15.549 %	3415	2998	-12.211 %
		360000	2435	2064	-15.236 %	2751	2425	-11.850 %
		380000	2066	1759	-14.860 %	2242	1985	-11.463 %

The amount of difference is decreasing or increasing gradually resembling a gradual second degree polynomial. One explanation for this could be that formulation for contact stiffness only considers the geometry of the contact and there is this one loading condition where stiffness value is the most correct. This shortcoming could be remedied by introducing a contact stiffness formulation that includes the influence of loading as well.

Difference amount of ball bearings is also much lower than roller bearings. This could be due to the simpler geometry in the ball bearing in comparison to that in the roller bearings. Since the actual geometries for bearings are not public knowledge, it could be that the estimation formulas for ball bearings are more accurate than the ones for roller bearings.

When looking at the results for RRB, we can see that the difference percentage for spherical roller bearing 23056-BE-XL is very high, approximately 50 %. The loading level of 15 000 N was taken into closer examination and there were differences in the contact pressures between the Python application and BearinX. To remove this difference, the contact pressures were extracted from BearinX instead and then used as input in the Python application. However, even with this modification there was still an difference of 15 %. This number could be lower by changing any of the approximated parameters, such as effective roller length L_{we}, but obviously this is not a sound solution just to adjust the inputs to match the results.

This reveals the flaw with the ISO 16281 model of calculation. As we can't get an accurate input values there is a situation of *"garbage in, garbage out"* with the model. Thus the verification, at least on the part of roller bearings is very difficult unless accurate input values can be sourced. If we can't have uniform input values, it is impossible to say which of the differences are induced by the errors in the application and which ones by the inaccurate input values.

5.2 Shaft Tool Verification

The shaft tool programmed in Python was verified against TEData MDESIGN DIN 743 model. As DIN 743 standard only supports safety factor calculations, we were unable to compare damage numbers between the software and the Python code. Material was selected as S355N structural steel [29] and number of cycles was 500 for each load case.

Calculations were performed on a shoulder depicted in Figure 17.

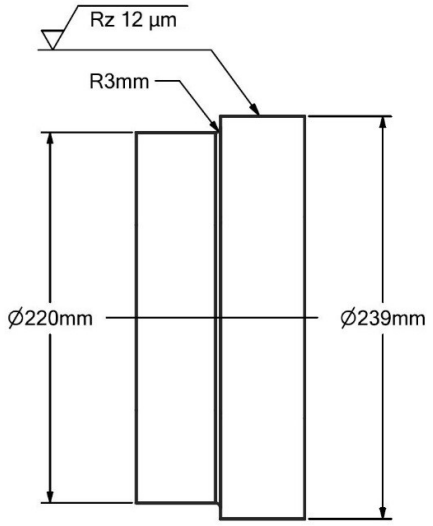

d_{eff}	239 mm
D	239 mm
d	220 mm
r	3 mm
R_z	12 µm

Figure 17. *Verification shoulder*

For the shaft shoulder fatigue stress limits, mean stress influence factors and yield points were calculated such as they are in Table 16.

Table 16. *Shoulder values*

$\psi_{zd\sigma K}$	0.088	
$\psi_{b\sigma K}$	0.095	
$\psi_{\tau K}$	0.080	
σ_{zdWK}	69.552	MPa
σ_{bWK}	74.099	MPa
τ_{tWK}	63.346	MPa
σ_{zdFK}	301.839	MPa
σ_{bFK}	362.207	MPa
τ_{tFK}	190.109	MPa

Safety factors were then calculated for nine different load cases. In first three load cases loading is fairly consistent and it fluctuates slightly between load cases. In the middle group one direction is loaded heavily and others are nominally loaded. In the last three mean loads are the same as in load case 1 while amplitude was increased until some amount of damage was accumulated and then the amplitude for each loading direction was increased by 5 MPa per load case.

Table 17. *Result for loading cases from MDESIGN and Python*

LC	σ_{zda} (MPa)	σ_{zdm} (MPa)	σ_{ba} (MPa)	σ_{bm} (MPa)	τ_{ta} (MPa)	τ_{tm} (MPa)	S_C (MDESIGN)	S_C (Python)	Diff (%)	Damage (Python)
1	15	40	10	15	20	30	1.511	1.511	0.00 %	0.000000
2	20	30	15	40	10	15	1.360	1.360	0.00 %	0.000000
3	10	15	20	30	15	40	1.320	1.319	-0.08 %	0.000000
4	40	50	5	5	5	5	1.196	1.196	0.00 %	0.000000
5	5	5	40	50	5	5	1.198	1.197	-0.08 %	0.000000
6	5	5	5	5	40	50	1.121	1.120	-0.09 %	0.000000
7	30	40	25	15	35	30	0.879	0.879	0.00 %	0.001065
8	35	40	30	15	40	30	0.771	0.771	0.00 %	0.002304
9	40	40	35	15	45	30	0.686	0.686	0.00 %	0.004543

The outputs from the Python program appear almost identical to those from MDESIGN as we can see in Table 17. In some cases, there are minor differences in the results as the Python program is giving slightly lower results. This could be due to differences in the rounding schemes between the programs or some slight differences in the inputs. Damage predicted by the Python program also behaves as expected since before our safety factors go below 1, we are not accumulating any damage. Increase in the amplitudes also results in higher damages as expected.

6. CONCLUSIONS

The goal of this master's thesis project was to create component fatigue modeling programs as part of a digital twin to predict remaining useful lifetime in a condition monitoring setting. The two components chosen for the scope were bearings and shafts. The bearing calculation program was based on ISO 281 standard and ISO TS 16281 technical specification, and the shaft program was based on DIN 743 standard.

The ISO standards for bearings proved well suited for a digital twin integration, because the standard calculation outputs cycle numbers instead of safety factors. With these fatigue life cycle limits it is easy calculate damage for each bearing based on measured load levels and loading cycles. Implementation of basic calculation defined in ISO 281 was straight forward as all the information needed to perform the calculation is readily available. With the refence calculation of ISO TS 16281, the most problematic part was the calculation of contact line pressures. A few different techniques we research, but eventually the alternative slicing technique of R. Teutsch, B. Sauer was selected due to ease of implementation, lower computation time and being able to solve in 2D. The calculation of the contact line pressure was not successful during this thesis due to the contact geometry being considered proprietary information by the manufacturers and approximations not providing accurate results.

In the future, it could be discussed with the manufacturers, if they would be more willing to generate the contact line pressures, since these are usually outputted by their own calculation tools. These pressure results could then be used to make the reduced order model for each bearing. Additionally, when the digital twins are deployed on live thrusters, whether the basic model or the more advanced reference model is more suited for the environment should be studied.

The shaft fatigue calculation using the DIN 743 had two major obstacles that needed to be solved, counting the input loading cycles from three different load directions and transforming the safety factor output into damage. Because of the time constrains with the project, we chose to use a third party library for single axis rainflow counting. The counting for the three different directions was done in ten second blocks to retain relative synchronicity between the different directions, instead of doing the whole signal at once. Secondly, the S-N curves in DIN 743 were defined separately for each loading direction and the standard doesn't provide a fatigue damage calculation method for combined loading state. Since calculating the safety factor was the option for combined loading state calculation, the defined S-N curves were combined and modified from the conventional stress-cycle definition to safety factor-cycle definition. This we are able to extract the limiting number of cycles from the S-N curves even when calculating fatigue safety factor without using an iterative approach.

Currently the biggest gain in the shaft fatigue module is seen in improving the rainflow calculation to provide more accurate loading cycles to the standard calculation. One approach could be implementing the modified Wang-Brown method which uses reduced dimensional state to calculate cycles for a multidirectional loading. Another way could be to combine the three directions into some sort of signed combined stress so we could use the single axis rainflow. This approach would require the combined stress points to programmatically store the original values or have some way to decouple the combined state so we could have the three directions required to feed the shaft calculation.

REFERENCES

[1] Petrodata Offshore Rig Day Rate Trends, IHS Markit, Available (accessed on Feb 15. 2019): https://ihsmarkit.com/products/oil-gas-drilling-rigs-offshore-day-rates.html

[2] T. M. Allen, U.S. Navy Analysis of Submarine Maintenance Data and the Development of Age and Reliability Profiles, Department of the Navy SUBMEPP, 14 p.

[3] S. J. Lacey, An Overview of Bearing Vibration Analysis, Maintenance & Assent Management, Vol. 23, No. 6, Dec 2008, pp. 32-42

[4] ISO 15243:2004(E), Rolling bearings — Damage and failures — Terms, characteristics and causes, 1st edition, International Organization for Standardization, Feb 15. 2004, 41 p.

[5] H. Nguyen-Schäfer, Computational Design of Rolling Bearings, Springer, 2016, 235 p.

[6] T. A. Harris, M. N. Kotzalas, Rolling Bearing Analysis: Essential Concepts of Bearing Technology, 5th edition, CRC Press LLC, Oct 9. 2006, 392 p.

[7] T. A. Harris, M. N. Kotzalas, Rolling Bearing Analysis: Advanced Concepts of Bearing Technology, 5th edition, CRC Press LLC, Oct 9. 2006, 370 p.

[8] ISO 281:2007(E), Rolling bearings — Dynamic load ratings and rating life, 2nd edition, International Organization for Standardization, Feb 15. 2007

[9] G. Lundberg, A. Palmgren, Dynamic Capacity of Rolling Bearings, Acta Polytechnica: Mechanical Engineering Series, Vol. 1, No. 3, 1947, pp. 1-50

[10] G. Lundberg, A. Palmgren, Dynamic Capacity of Rolling Bearings, Acta Polytechnica: Mechanical Engineering Series, Vol. 2, No. 4, 1952, pp. 1-32

[11] W. Weibull, A Statistical Theory of the Strength of Materials, IVA Handlingar, Vol. 151, 1939, pp. 1-45

[12] W. Weibull, The Phenomenom of Rupture in Solids, IVA Handlingar, Vol. 153, 1939, pp. 1-55

[13] Basic dynamic load rating, C, SKF, Available (accessed on Jun 11. 2019): https://www.skf.com/us/products/bearings-units-housings/principles/bearing-selection-process/bearing-size/size-selection-based-on-rating-life/basic-dynamic-load-rating/index.html

[14] ISO/TR 1281-1:2008(E), Rolling bearings — Explanatory notes on ISO 281 — Part 1: Basic dynamic load rating and basic rating life, 1st edition, International Organization for Standardization, Dec 1. 2008, 40 pp.

[15] ISO/TR 1281-2:2008(E), Rolling bearings — Explanatory notes on ISO 281 — Part 2: Modified rating life calculation, 1st edition, based on a systems approach to fatigue stresses, International Organization for Standardization, Dec 1. 2008, 47 p.

[16] ISO 281:2007 bearing-life standard - and the answer is?, Tribology & Lubrication Technology, Vol. 66, STLE, No. 7, Jul 1. 2010, pp. 34-43

[17] E. Ioannides, G. Bergling, A. Gabelli, An Analytical Formulation for The Life of Rolling Bearings, Acta Polytechnica Scandinavia: Mechanical Engineering Series, Vol. 137, 1999, pp. 1-80

[18] E. Ioannides, T.A. Harris, A New Fatigue Life Model for Rolling Bearings, Journal of Tribology, Vol. 107, American Society of Mechanical Engineers, Jul 1985, pp. 367-378

[19] A. Palmgren, Ball and Roller Bearing Engineering, 3rd edition, SKF, 1959, 264 pp.

[20] A. Hoeg, ISO 4406: What Do Those Numbers Mean in the ISO Cleanliness Codes?, Hy-Pro Filtration, Oct 8. 2012, Available (accessed on Jun 17. 2019): https://info.hyprofiltration.com/blog/bid/216397/ISO-4406-What-do-those-numbers-mean-in-the-ISO-Cleanliness-Codes

[21] ISO/TS 16281:2008(E), Rolling bearings — Methods for calculating the modified reference rating life for universally loaded bearings, 1st edition, International Organization for Standardization, Jun 15. 2008, 20 pp.

[22] J. Kiefer, Sequential minimax search for a maximum, Proceedings of the American Mathemactical Society, Vol. 4, 1953, pp. 502-506

[23] M. J. Hartnett, A General Numeric Solution for Elastic Body Contact Problems, Solid Body Contact and Lubrication, Winter Annual Meeting of the American Society of Mechanical Engineers, ASME, Nov 1980, pp. 51-66

[24] R. Teutsch, B. Sauer, An Alternative Slicing Technique to Consider Pressure Concentrations in Non-Herzian Line Contacts, Journal of Tribology, Vol. 126, No. 3, ASME, Jul 2004, pp. 436-442

[25] TI No. WL 43-1190 EA, Technical Information, FAG Rolling Bearings: Fundamental, Types, Designs, FAG, 1997, 55 pp.

[26] M. A. Miner, Cumulative Damage in Fatigue, Journal of Applied Mechanics, Vol. 12, ASME, 1945, pp. 159-164

[27] DIN 743-1:2012-12, Calculation of load capacity of shafts and axles – Part 1: General, English translation of DIN 743-1:2012-12, DIN Deutsches Institut für Normung, Dec 2012, 25 pp.

[28] DIN 743-2:2012-12, Calculation of load capacity of shafts and axles – Part 2: Theoretical stress concentration factors and fatigue notch factors, English translation of DIN 743-2:2012-12, DIN Deutsches Institut für Normung, Dec 2012, 34 pp.

[29] DIN 743-3:2012-12, Calculation of load capacity of shafts and axles – Part 3: Strength of materials, English translation of DIN 743-3:2012-12, DIN Deutsches Institut für Normung, Dec 2012, 8 pp.

[30] DIN 743-4:2012-12, Calculation of load capacity of shafts and axles – Part 4: Fatigue limit, endurance limit – Equivalently damaging continuous stress, English translation of DIN 743-4:2012-12, DIN Deutsches Institut für Normung, Dec 2012, 11 pp.

[31] B. McGinty, Von Mises Stress, www.continuummechanics.org, Available (accessed on Jul 31. 2019): http://www.continuummechanics.org/vonmisesstress.html

[32] R. von Mises, Mechanik der festen Korper im plastisch-deformablen Zustand, Nachrichten von der Gesellschaft der Wissenschaften zu Göttingen, Vol. 1, Mathematisch-Physikalische Klasse, 1913, pp. 582-592

[33] R. E. Peterson, Stress Concentration Factors, John Wiley & Sons, 1974, 317 pp.

[34] Y. Lee, M. E. Barkey, H. Kang, Metal Fatigue Analysis Handbook: Practical Poblem-Solving Techniques fro Computer-Aided Engineering, Butterworth-Heinemann, 2012, 580 pp.

[35] M. Matsuishi, T. Endo, Fatigue of Metal Subjected to Varying Stress, Japan Society of Mechanical Engineers, 1968

[36] S. D. Downing, D. F. Socie, Simple Rainflow Counting Algorithm, International Journal of Fatigue, Vol. 4, No. 1, Butterworth & Co, Jan 1982, pp. 31-40

[37] ASTM E 1049-85 (Reapproved in 2017), Standard Practices for Cycle Counting in Fatigue Analysis, ASTM International, 1985, 10 pp.

[38] M. A. Meggiolaro, J. T. P. de Castro, An improved multiaxial rainflow algorithm for non-proportional stress or strain histories – Part I: Enclosing surface methods, International Journal of Fatigue, Vol. 42, Elsevier, Sep 2012, pp. 217-226

[39] M. A. Meggiolaro, J. T. P. de Castro, An improved multiaxial rainflow algorithm for non-proportional stress or strain histories – Part II: The Modified Wang–Brown method, International Journal of Fatigue, Vol. 42, Elsevier, Sep 2012, pp. 194-206

[40] Medias - Schaeffler Online Catalogue, Schaeffler, Available (accessed Nov 10. 2019): https://medias.schaeffler.com/medias/

[41] History.com Editors, Industrial revolution, A&E Television Network, Available (accessed Jul 23. 2020): https://www.history.com/topics/industrial-revolution/industrial-revolution

[42] E. Niiler, How the Second Industrial Revolution Changed Americans' Lives, A&E Television Network, Available (accessed Jul 23. 2020): https://www.history.com/news/second-industrial-revolution-advances

[43] C. Salkin, M. Oner, A. Ustundag, E. Cevikcan, Industry 4.0: Managing the Digital Transformation, Chapter 1: A Conceptual Framework for Industry 4.0, Springer, 2018, pp. 3-23

[44] S. Boschert, R. Rosen, Mechatronic Futures, Chapter 5: Digital Twin – The Símulation Aspect, Springer, 2016, pp. 59-74

[45] R. Rosen, G. von Wichert, G. Lo, K.D. Bettenhausen, About the Importance of Autonomy and Digital Twins for the Future of Manufacturing, IFAC-PapersOnLine 48-3, Elsevier, 2015, pp. 567-572

[46] Taking flight with the Airbus “Iron Bird”, Airbus, Available (accessed Jul 23. 2020): https://www.airbus.com/newsroom/news/en/2017/05/taking-flight-with-the-airbus-iron-bird.html

[47] M. Grieves, Digital Twin: Manufacturing Excellence Through Virtual Factory Replication, Michael W. Grieves LLC, 2015, 8pp.

[48] J. Thilmany, Identical Twins, ASME, Sep. 2017, Available (accessed Aug 16. 2020): https://www.asme.org/topics-resources/content/identical-twins

[49] M. Shafto et al., DRAFT Modeling, Simulation Information Technology & Processing roadmap, Technology Area 11, NASA, Nov. 2010 32 pp.

[50] E. H. Glaessgen, D. S. Stargel, The Digital Twin Paradigm for Future NASA and U.S. Air Force Vehicles, 53rd Structures, Structural Dynamics and Materials Confrerence, Apr. 2012, 14 pp.

[51] A. Sandberg, N. Bostrom, Whole Brain Emulation: A Roadmap, TechnicalReport #2008-3, Appendix B: Computer Performance Development, Future of Humanity Institute, Oxford University, 2008, pp. 86-100

[52] S. J. Lacey, An Overview of Bearing Vibration Analysis, Maintenance & Asset Management, Vol. 23, No. 6, Nov 2008, pp. 32-42

[53] S. C. Shorten, Machinery Condition Monitoring, Why has the shipping industry been slow to adopt?, Lloyd's Register EMEA, Technical Investigations Department, UK, 2012, 12 pp.

[54] G. A. Susto, A. Schirru, S. Pampuri, Machine Learning for Predictive Maintenance: A Multiple Classifier Approach, IEEE transactions on industrial informatics, Vol.11, No. 3, Jun 2015, pp. 812-820

[55] C. F. Adams, Notes on Railroad Accidents, Putnam, 1879, 280 pp.

[56] C. Bathias, A. Pineau, Fatigue of Materials and Structures - Fundamentals. John Wiley & Sons, 2010, 505 pp.

[57] R. A. Smith, The Versailles railway accident of 1842 and the first research into metal fatigue, Fatigue'90, vol. IV, EMAS, Birmingham, 1990, p. 2033-2041

[58] G. M. Teixeira, Fatigue of Metal: Failure and Success, Dassault Systems, May 2017, 10 pp.

[59] R. P. Reed, J. H. Smith, B. W. Christ, The Economic Effects of Fracture in the United States, National Bureau of Standards, Mar 1983

[60] N. E. Dowling, Mechanical Behavior of Materials, 4th Edition, Pearson Education Ltd., Mar 2012, 960 pp.

[61] W. Schütz, A History of Fatigue, Engineering Fracture Mechanics, Vol. 54, No. 2, Elsevier Science Ltd., 1996, pp. 263-300

[62] A. Morin, Lemons de mécanique practique - résistance des matériaux, Librairie de L. Hachette et Cie, 1853, p. 456

[63] O. H. Basquin, The Exponential Law of Endurance Tests, Proceedings of Annual Meeting of American Society for Testing Materials, Vol. 10, 1910, pp. 625-630

[64] A. Palmgren, Die Lebensdauer von Kugellagern. VDI-Zeitschrift 68, 1924, pp. 339-341